CONCEPTUAL DESIGN OF ROTATING WIRE SYSTEM WITH BUCKING USING MULTICHANNEL LOCK-IN AMPLIFIER

Yung-Chuan Chen

Submitted to the faculty of the University Graduate School

in partial fulfillment of the requirements

for the degree

Master of Science

in the Department of Physics,

Indiana University

December 2018

Accepted by the Graduate Faculty, Indiana University, in partial fulfillment of the requirements for the degree of Master of Science.

Master's Thesis Committee

Dr. W. Michael Snow

Dr. Rex Tayloe

Ronald Agustsson

December 10, 2018

ACKNOWLEDGMENTS

First, I would like to thank my supervisor Ronald Agustsson, Salime Boucher, and Alex Murokh and my generous employer Radiabeam Technologies to support me through USPAS sessions and the Master's degree. All these supports from material, spiritual, and knowledge perspective make me being here to defend my Master's thesis. I'm really grateful for Indiana University to offer and continue offering the Master degree program, so I can be in advanced academic system again from an employment in industry. I would like to thank Dr. W. Michael Snow for being the chair and Dr. Rex Tayloe for being the member of my master's committee. I also want to thank Susan Winchester and Nelson Batalon to keep track on my enrollment and degree progress. I hope USPAS and IU master program continue training new scholars and engineers and hope the best to people in this program to pursue their degree.

Yung-Chuan Chen

CONCEPTUAL DESIGN OF ROTATING WIRE SYSTEM WITH BUCKING USING MULTICHANNEL LOCK-IN AMPLIFIER

Quality assurance in accelerator magnet is important to ensure functionality of accelerator and quality of experiment data. The quality of magnet is determined by the harmonic content, which can be measured accurately and efficiently by rotating coil method. In this thesis, the theory of rotating coil method is thoroughly discussed. The derivation starts with multipole expansion of magnetic field in cylindrical coordinate. A harmonic decomposition method is introduced to calculate harmonic content from field map. By induction, change of flux in time is sensed by coil during rotation. After analysis, harmonic content is acquired from sinusoidal voltage signal. The accuracy of harmonic content degrades due to error in signal strength, timer, angular position, coil geometry, inconsistent speed and vibration. These errors can be suppressed by calibration, time integration, and bucking. The rotating wire approach in Argonne National Laboratory is adopted because of its simplicity and flexibility. Challenges in low signal strength and shaft-free rotation mechanism are solved by lock-in amplifier and synchronized rotary stages. The proposed system is further improved with bucking capability for two harmonics simultaneously. Based on hardware specification, manufacture error, operating parameters, and calibration source, the accuracy and precision of proposed system are 0.1% and 25ppm, respectively, after proper calibration and alignment. Estimated time for single scan is 15 seconds.

CONTENTS

CHAPTER 1

INTRODUCTION

In beam dynamic, particle's transverse motion is controlled by magnetic field. Magnetic field controls more than just ideal beam trajectory, but also particles' motion with respect to ideal trajectory. The properties to describe these beam behaviors are called beta function, chromaticity, and tune shift,. . . , etc. Different types of magnet are designed to generate fields that provide accurate bending, focusing, and correction for dynamic errors. These magnets are categorized by the number of poles, such as dipole, quadrupole, sextupole,. . . , 2n-pole magnets.

Theoretically, 2n-pole magnet only generates 2n-pole field, or so called nth harmonic field. The ideal harmonic field required infinite geometry and only exist in 2D domain. In reality, a magnet designed for nth harmonic field must contain other harmonic fields. With proper design, the field impurity can be suppressed to certain acceptable level. If the product magnet doesn't fulfill the specification, the system cannot deliver the promised accuracy or the entire experiment might not even run. Measurement is necessary on magnets.

The main property to characterize the quality of magnet is the harmonic content. This information is most commonly expressed as the strength of fundamental harmonic(s) and the ratio between other harmonics and the fundamental harmonic(s). The former describe the strength of purposed treatment on beam and the latter describe the relative level of

mistreatment on beam. For simplicity, the magnet in this thesis is assumed to have only one fundamental harmonic.

For magnets with adjustable strength, the quality requirement can be extended to harmonic content at different operating conditions. These conditions can have different beam energy (hysteresis measurement), different time (dynamic measurement for AC and pulsed magnet), different temperature (center shift due to thermal expansion), or being at off-condition (remnant measurement). The total number of measurements can easily scale up. Therefore, the efficiency in measurement needs great consideration.

In some cases, fundamental harmonic(s) can be the only value to control for certain magnets that are more forgiving. For example, the dipole field strength capability may be the only considered requirement for steering magnet. For this case measurement can be as simple as several field vs distance scans parallel to beam trajectory, measured at different operating condition.

Based on physical principles, the measurement method for magnetic field can be categorized into induction, Lorentz force, hall effect, and magnetic resonance. Each method has its strong and weakness. A good summary of these methods are worked out in other article [1] [2].

Except magnetic resonance method, all these measurement method are workable for harmonic content. The analysis for harmonic content is discussed in later section. Because the analysis is based on result of integrated field in axial direction at different azimuthal angle, rotating coil would be the most efficient way, as the raw data is already integrated in axial direction. However, the pre-integrated raw data also means the loss of local field information. If local field (for example, at magnet entrance or shim location) is interested, it needs to be measured by hall probe or a shorter version of rotating coil.

Table 1.1: Measurement method and associated physical principle

Physical principle	Methods
Induction	Fixed coil, Rotating coil, stretch wire
Lorentz force	Pulse wire, vibrating wire
Hall effect	Hall probe
Magnetic resonance	NMR probe

1.1 ROTATING COIL METHOD

Rotating coil method takes advantage of Faraday's Law to measure field information and angular position dynamically. A conductor coil is exposed to certain amount of magnetic flux at an angular position. As the coil rotates at constant known speed, the changing magnetic flux induces voltage signal in time domain that gets digitized by analog-to-digital converter. Normally, the voltage signal needs to be integrated in time so it becomes magnetic flux which contains magnetic field information. Meanwhile, the angular position in time domain is recorded by rotary encoder. The resulting flux versus time data is then translated into flux versus angle data to perform harmonic analysis.

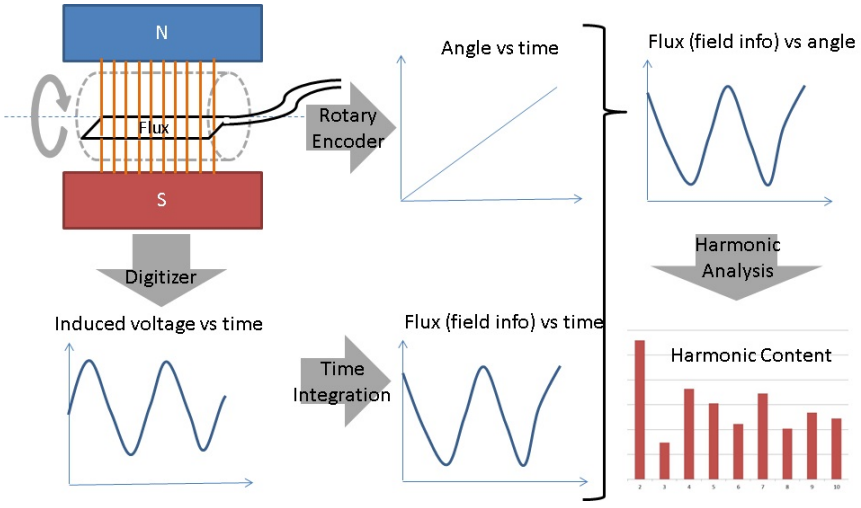

Figure 1.1: Schematic of rotating coil method

The major limiting factors of a rotating coil system are signal resolvability, calibration, and rotation purity. These factors are related to limitation of hardware and coil manufacture. We can classify and quantify different systems by their coil design, bucking capability, accuracy, precision, and repeatability.

- Coil design: The coil can be single loop or multiple loops that are perpendicular or parallel with respect to rotating direction. Coil geometry and configuration effects the strength of induced voltage signal. Different coil fixture changes manufacture process and has different manufacture tolerance.
- Bucking capability: The coil of multiple loops can be arrange in a special way to nullify (buck) its ability to measure one or more harmonic so the other harmonic can be measured correctly. Detail is discussed in later section.
- Accuracy: The correctness of measurement result relies on the overall systematic error. The accuracy gives the range of actual harmonic content with respect to measurement. Accuracy can be improved by calibration if necessary, but it can only be as good as the accuracy of calibration source.
- Precision: The data acquisition device has minimum resolvable signal strength based on noise and random error. It gives a minimum resolvable harmonic content of measurement result. The digits below precision are meaningless and should be abandoned. If one harmonic is measured lower than precision, that harmonic is not resolvable.
- Repeatability: The consistency of multiple measurements is also based on random error and noise. Repeatability gives the confidence of measurement result and the system itself. It should reflect the precision of system and consequently determine if the commission succeeds or not.

1.2 EXAMPLE QUADRUPOLE MAGNET: EMQD-280-709

There are 10 quadrupole magnet products made by Radiabeam Technologies for Integrable Optics Test Accelerator (IOTA) at Fermilab. They are measured with 3D hall probe system in Radiabeam Technologies, Santa Monica. The 3D field map consists of 12 points per slice and 81 slices and it is just enough data to resolve harmonic content up to 6th harmonic. The repeatability of motion stage limits the maximum number of data point. The accumulated shift in position can caused erroneous result in dipole harmonic. Each measurement takes about 4 hours to complete after alignment. For 10th harmonic, the estimated scan time would be 8 hours. With rotating coil, the measurement time can be a lot shorter. Higher order harmonic can be measured. Precision can be improved by redundant measurement too.

To validate harmonic content more accurately and efficiently, a rotating coil system is keenly considered. Based on survey of existed system and the capability at Radiabeam Technologies, a rotating wire system with bucking capability is proposed. To make the designing work practical, EMQD-280-709, a diamond shape quadrupole magnet, is chosen as a measurement target. A coil is designed for this magnet to explore the limit of the system.

Table 1.2: Design value and hall probe measurement result of EMQD-280-709, serial # FNM1_01

Properties	**Unit**	**Design value**	**Measured value**
Reference radius (r_0)	[mm]	24	24
B'	[T/m]	5.979	5.886
B_2 at r_0	[T]	0.143	0.141
Magnetic length	[m]	0.211	0.210

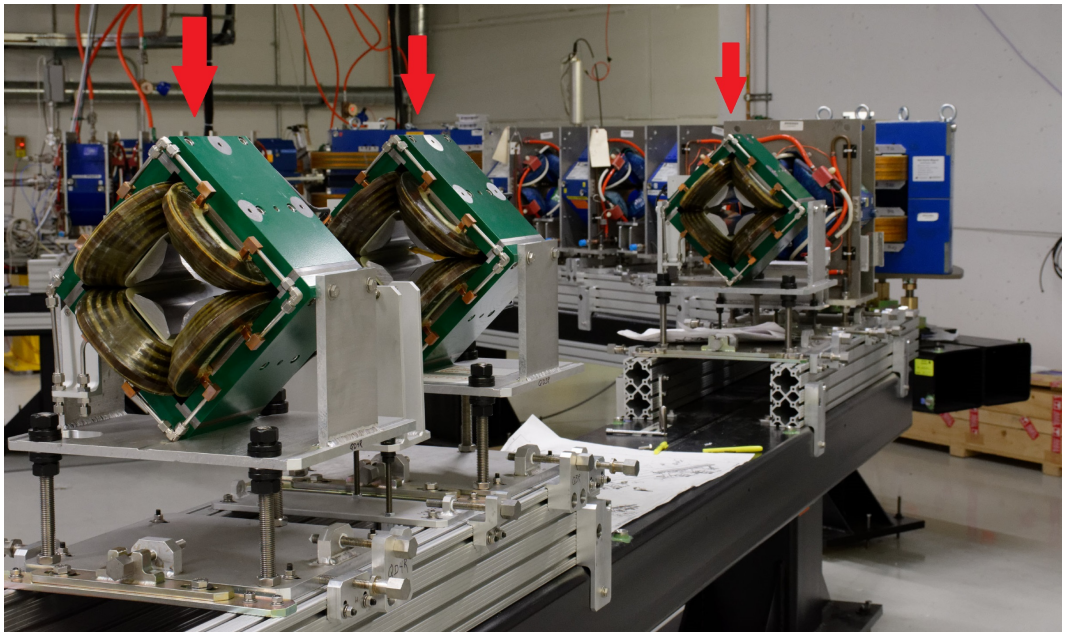

Figure 1.2: Picture of EMQD-280-709 quadrupole magnet for IOTA at Fermilab.

Table 1.3: Harmonic content of EMQD-280-709, serial # FNM1_01. Hall probe measurement

	Design				**Measurement (up to n=6)**			
n	Int. Bn	Int. An	Int. Cn	Skew angle	Int. Bn	Int. An	Int. Cn	Skew angle
	[Unit]	[Unit]	[Unit]	[rad]	[Unit]	[Unit]	[Unit]	[rad]
1	0	0	0	0	-4	8	9	-2.040
2	10000	0	10000	0	10000	1	10000	0.000
3	0	0	0	3.04	1	3	3	-1.370
4	1	0	1	0.0001	-5	4	7	-2.390
5	0	0	0	0.0322	0	-1	1	1.040
6	26	0	26	0	5	-2	6	0.309
7	0	0	0	-0.219	-	-	-	-
8	0	0	0	3.14	-	-	-	-
9	0	0	0	-2.96	-	-	-	-
10	-1	0	1	-3.14	-	-	-	-

CHAPTER 2

TECHNOLOGY SURVEY OF ROTATING COIL METHOD

There are many variations of rotating coil method due to improvement of data acquisition method and coil production precision. Table 2.1 shows some rotating coil system design and their measurement specification. Four systems are discussed based on author's interest. The coil design, bucking capability, accuracy, and repeatability are based on available publications. [3] [4] [5] [6] [7]

Table 2.1: List of rotating coil system, coil design, bucking, accuracy, and repeatability based available publications.

Facility	Coil design	Bucking	Accuracy	Repeatability(1 sigma)
			[unit]	[ppm]
BNL	5-Tangential	1^{st}, 2^{nd}	<5(before calibration)	<26 (up to n=3)
CERN	Tangential	1^{st}	0.41(dipole only)	100 (dipole only)
Fermilab*	Radial (PCB)	1^{st}, 2^{nd}	-	20 (up to n=7)
ANL	Radial (Wire)	None	0.5	-

*Collaboration work among Fermilab, CERN, and PSI [8]

2.1 TANGENTIAL COIL AT BNL, DIGITAL BUCKING

Brookhaven national laboratory (BNL) has tangential coil with traditional winding. However, each coil is digitized by separated channels. The signal can be manipulated by a bucking ratio before bucking applies. This extra freedom allows the sensitivity for each coil to be any number as long as the signal to noise ratio is decent enough. The beauty is that coil geometry and number of turns can be chosen at any workable combination.

In this merit, BNL comes up with a 5-tangential coil for RHIC quadrupoles and an upgraded 9-Tangential coil. All coils are wound on the groove of G-10 cylinder with a maximum of only 36 turns. The 5-tangential coil can measure harmonics from dipole to 12-pole except Octupole [9], with active dipole and quadrupole bucking. The 9-tangential coil can measure all harmonic, with active bucking up to any three harmonic [10].

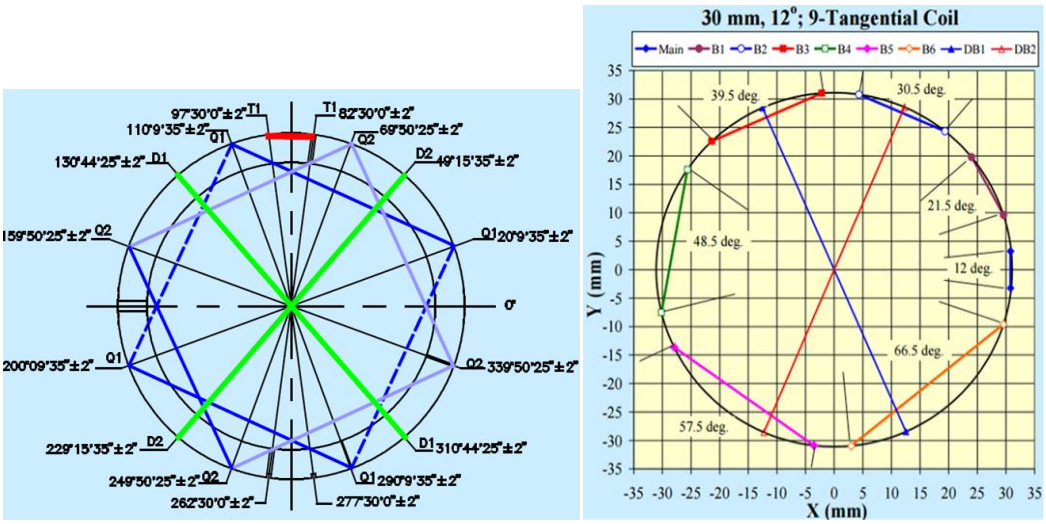

Figure 2.1: BNL 5-Tangential coil winding diagram [9] (Left). BNL 9-Tangential coil winding diagram [10] (Right)

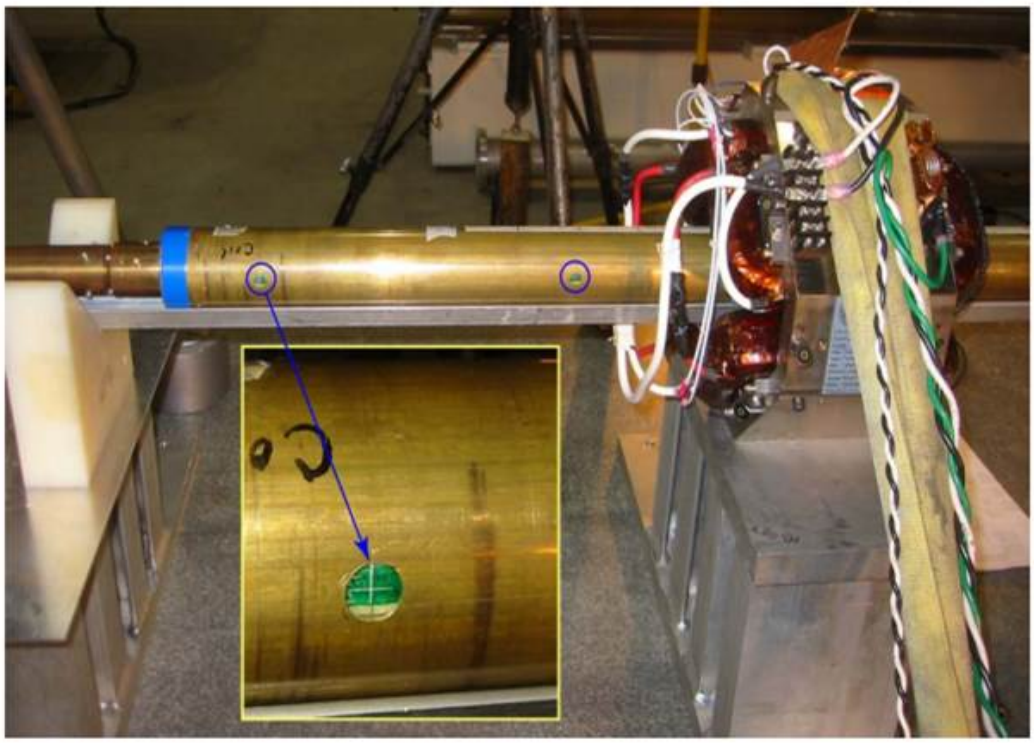

Figure 2.2: BNL 5-Tangential coil during calibration. [3]

2.2 ROTATING COIL FIELD MAPPER AT CERN

Traditional rotating coil requires straight through access. For access restricted magnets, say 90 degree bending dipole, the only applicable measurement technique is hall probe. However, hall probe in general has relatively worse accuracy. Therefore, a proof-of-principle field mapper rotating coil is developed at CERN for local field measurement. The rotating coil probe itself is calibrated to a reference dipole. The accuracy before calibration is 0.41 unit. The fringe field measurement has accuracy of 2%(worst case) between the mapper and hall probe measurement [4].

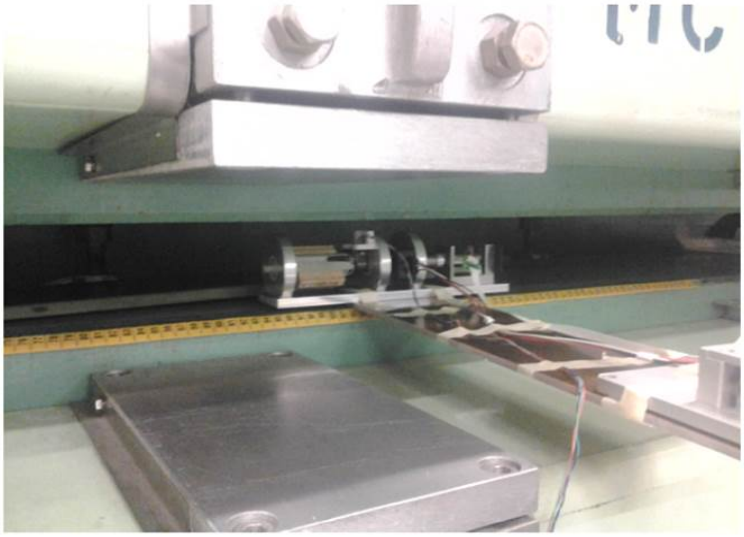

Figure 2.3: Rotating coil probe inside 1T reference dipole [4].

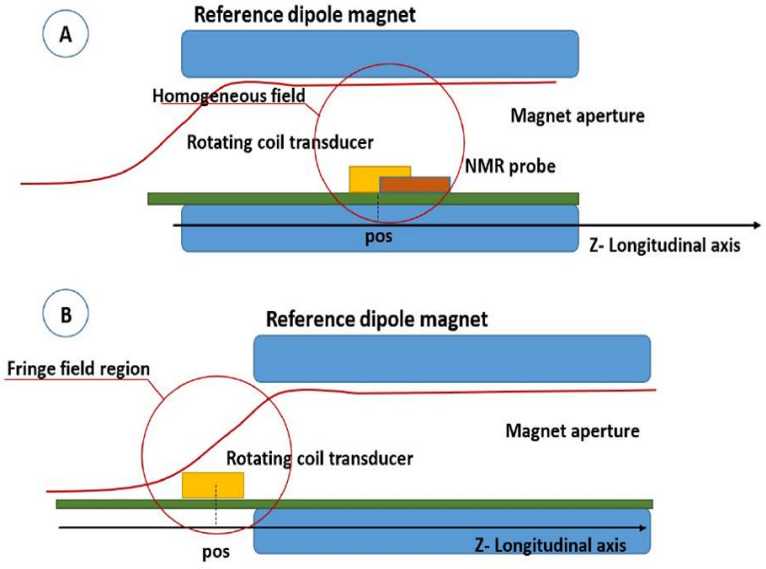

Figure 2.4: Schematic of rotating coil probe under testing for (a)accuracy and repeatability of main field (b) harmonic repeatibility of fringe field [4]

2.3 PCB COILS BY FERMILAB, CERN, AND PSI COLLABORATION

As precision of PCB production improved, it becomes popular in rotating coil development. It allows complicate geometry within tight positional tolerance. This is extremely practical for measuring small aperture magnet for Compact Linear Collider (CLIC). The coil sensitivity can be precisely calculated based on location of conductor position. With only 7.35mm diameter, it's able to measure quadrupole of 70T*m/m integrated gradient to 100ppm precision [5]. Assume the effective radius of coil is 8mm, the equivalent flux to pick up is as small as

$$70Tm/m * (0.007m)^2 * 100ppm = 3 * 10^{-7}weber.$$

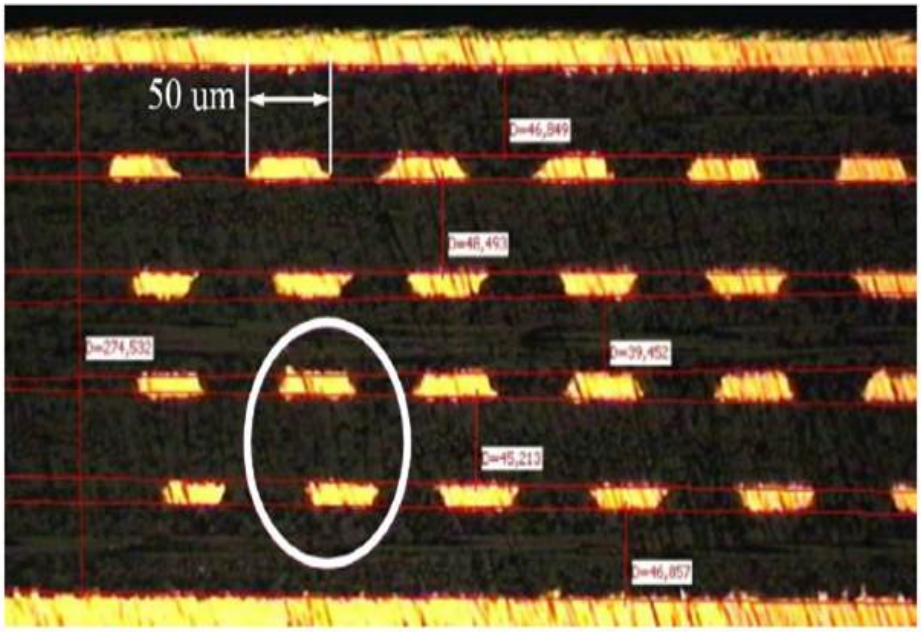

Figure 2.5: Cross-sectional view of Fermilab PCB coil for CLIC under microscope [5]

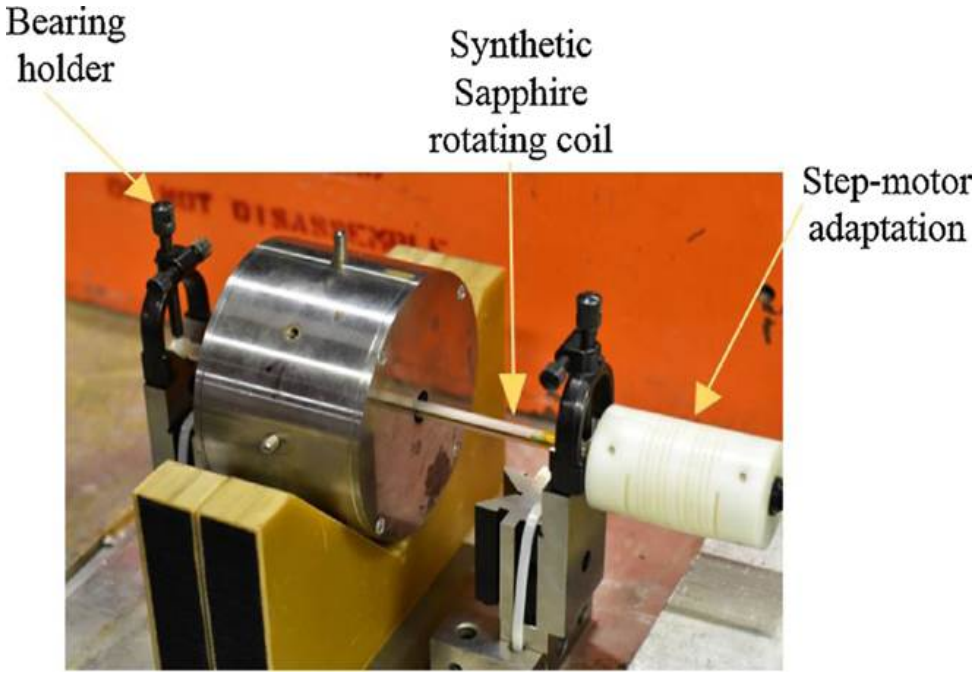

Figure 2.6: The Sapphire rotating coil is under calibration at Fermilab [5].

2.4 ROTATING WIRE AT ANL

The rotating wire approach is introduced at Argonne National Laboratory (ANL). The benefit of rotating wire is the adjustability in radial size and length. The measurement length makes multi-let magnet alignment feasible. A pair of rotary stage in synchronization is needed to make this shaft-free coil rotation possible.

The major issue in this approach is the poor signal to noise ratio. To overcome the noise, Lock-in amplifier is necessary to recover the signal by amplifying each harmonic individually. The drawback is the longer measurement time since data is collected for one harmonic at a time. Fortunately, rotating coil measurement is fast in general so the effect should be tolerable. The other drawback of this system is the lack of bucking. In this thesis, the proposed rotating wire system is modified with bucking capability using multichannel Lock-in amplification.

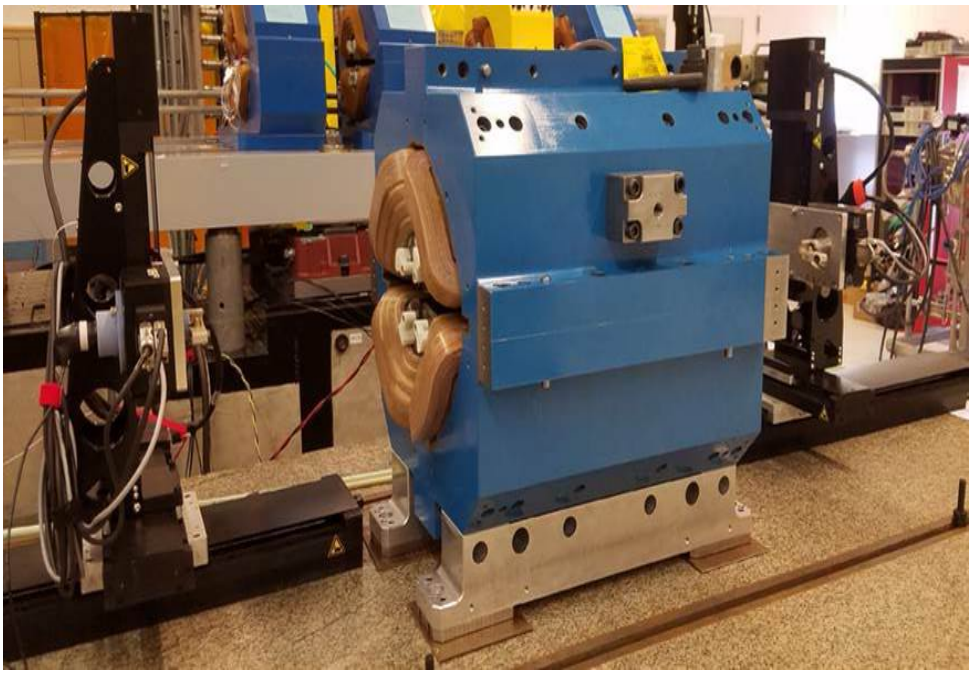

Figure 2.7: ANL rotating wire measuring APS quadrupole [6].

Figure 2.8: APS quadrupoles under alignment using ANL rotating wire [6].

CHAPTER 3

THEORY

3.1 MAGNETIC MULTIPOLE IN CYLINDRICAL COORDINATE

In a region free of current or magnetic material, the second and forth Maxwell equation can be written as:

$$\nabla \cdot \vec{B} = 0 \tag{3.1}$$

$$\nabla \times \vec{B} = 0 \tag{3.2}$$

Magnetic field satisfied equation 3.2 can be written as gradient of scalar potential:

$$\vec{B} = -\nabla F \tag{3.3}$$

Combined Equation 3.1 and Equation 3.3, we have the Laplace equation for magnetic potential:

$$\nabla^2 F = 0 \tag{3.4}$$

The solution is expressed in either Cartesian or cylindrical coordinate, where the z axis is parallel to beam trajectory. In two dimension (transverse direction), Equation 3.4 becomes:

$$\frac{\partial^2 F}{\partial r^2} + \frac{1}{r}\frac{\partial F}{\partial r} + \frac{1}{r^2}\frac{\partial^2 F}{\partial \theta^2} = 0 \tag{3.5}$$

Using separation of variable, the general solution of scalar potential is:

$$F(r,\theta) = \sum_{n=1} r^n \left[b_n \sin(n\theta) \ + a_n \cos(n\theta)\right] \tag{3.6}$$

where $b_n$and a_n are arbitral coefficient to be found out. From Equation 3.3, the magnetic field cylindrical components in 2D are derived:

$$B_r(r,\theta) = -\frac{\partial F}{\partial r} = -\sum_{n=1} n r^{n-1} \left[b_n \sin(n\theta) \ + a_n \cos(n\theta)\ \right] \tag{3.7}$$

$$B_\theta(r,\theta) = -\frac{1}{r}\frac{\partial F}{\partial \theta} = -\sum_{n=1} n r^{n-1} \left[b_n \cos(n\theta) \ - a_n \sin(n\theta)\right] \tag{3.8}$$

Using rotation matrix, the Cartesian components is derived as:

$$B_x(r,\theta) = -\sum_{n=1} n r^{n-1} \left[b_n \sin((n-1)\theta) \ + a_n \cos((n-1)\theta)\ \right] \tag{3.9}$$

$$B_y(r,\theta) = -\sum_{n=1} n r^{n-1} \left[b_n \cos((n-1)\theta) \ - a_n \sin((n-1)\theta)\ \right] \tag{3.10}$$

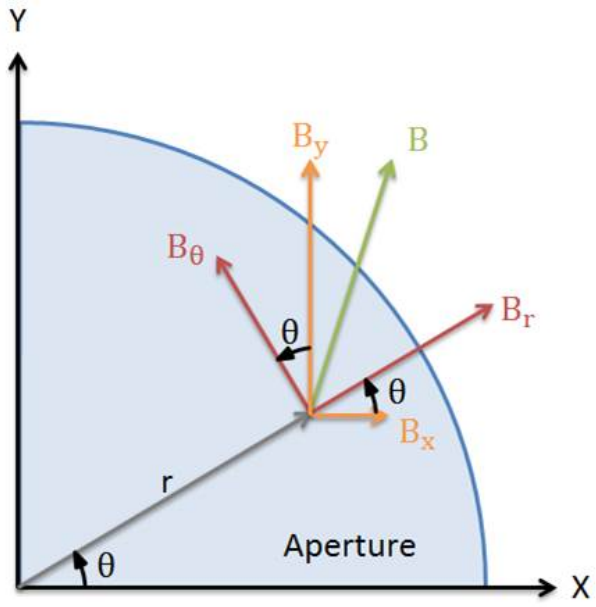

Figure 3.1: Illustration of Cartisian and cylindrical field component at position in cylindrical coordinate

The LHS of Equation 7 and Equation 8 has unit of field while coefficient $b_n$and $a_n$has unit of $\frac{field}{distance\ ^{n-1}}$. To make coefficients of different order comparable to each other, a new term is introduced to absorb the dependency of r^{n-1}.

$$\begin{pmatrix} B_n(r) \\ A_n(r) \end{pmatrix} = -nr^{n-1} \begin{pmatrix} b_n \\ a_n \end{pmatrix} \tag{3.11}$$

where $B_n(r)$ and $A_n(r)$ are magnitude of field at radial position r. B_n and A_n are in the unit of field (Tesla or Gauss). For clarification, reader should not get confused with coefficient B_n versus field component B_x, B_y, B_r, and B_θ. The magnitude of field at different radial position can be written in terms of magnitude of field at a reference radius r_0.

$$B_n(r) = \left(\frac{r}{r_0}\right)^{n-1} B_n(r_0) \tag{3.12}$$

$$B_r(r,\theta) = \sum_{n=1} \left(\frac{r}{r_0}\right)^{n-1} [B_n(r_0)\ \sin(n\theta)\ + A_n(r_0)\ \cos(n\theta)] \tag{3.13}$$

$$B_\theta(r,\theta) = \sum_{n=1} \left(\frac{r}{r_0}\right)^{n-1} [B_n(r_0)\ \cos(n\theta)\ - A_n(r_0)\ \sin(n\theta)] \tag{3.14}$$

For simplicity, B_n and A_n are used to stand for $Bn(r_0)$ and $An(r_0)$, as we keep in mind that they are the harmonic coefficient acquired at reference radius r_0. We acquire the multipole expansion form in cylindrical coordinate:

$$B_r(r,\theta) = \sum_{n=1} \left(\frac{r}{r_0}\right)^{n-1} [B_n \sin(n\theta)\ + A_n \cos(n\theta)] \tag{3.15}$$

$$B_\theta(r,\theta) = \sum_{n=1} \left(\frac{r}{r_0}\right)^{n-1} [B_n \cos(n\theta)\ - A_n \sin(n\theta)] \tag{3.16}$$

Using rotation matrix and simplify the sinusoidal functions, the Cartesian field component as function of r and θ can be acquired:

$$B_x(r,\theta) = \sum_{n=1} \left(\frac{r}{r_0}\right)^{n-1} [B_n \sin((n-1)\theta)\ + A_n \cos((n-1)\theta)] \tag{3.17}$$

$$B_y(r,\theta) = \sum_{n=1} \left(\frac{r}{r_0}\right)^{n-1} [B_n \cos((n-1)\theta)\ - A_n \sin((n-1)\theta)] \tag{3.18}$$

For dipole field (n=1), we have

$$\begin{cases} B_r(r,\theta) = B_1 \sin\theta \ + A_1 \ \cos\theta \\ B_\theta(r,\theta) = B_1 \cos\theta \ - A_1 \ \sin\theta \end{cases} \tag{3.19}$$

or

$$\begin{cases} B_x(x,y) = A_1 \\ B_y(x,y) = B_1 \end{cases} \tag{3.20}$$

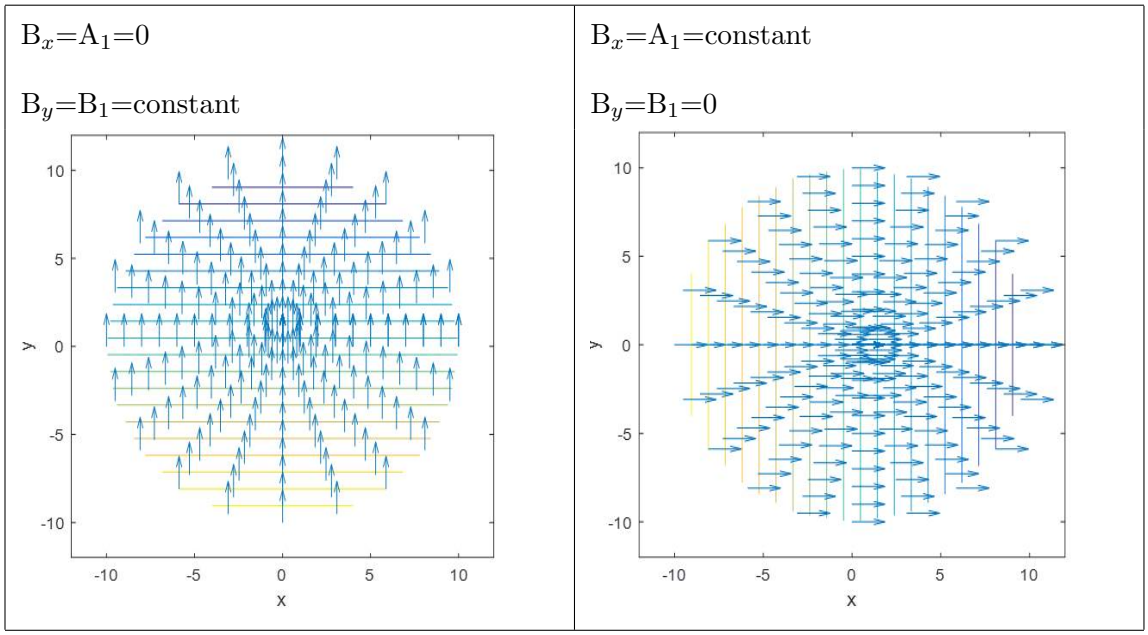

Figure 3.2: Field plot of upright dipole (left) and skew dipole (right)

For quadrupole field (n=2), we have

$$\begin{cases} B_r(r,\theta) = \left(\frac{r}{r_0}\right)[B_2 \sin 2\theta \ + A_2 \ \cos 2\theta] \\ B_\theta(r,\theta) = \left(\frac{r}{r_0}\right)[B_2 \cos 2\theta \ - A_2 \ \sin 2\theta] \end{cases} \tag{3.21}$$

or

$$\begin{cases} B_x(x,y) = \frac{1}{r_0}[B_2 y + A_2 \mathrm{x}] \\ B_y(x,y) = \frac{1}{r_0}[B_2 x - A_2 \ \mathrm{y}] \end{cases} \tag{3.22}$$

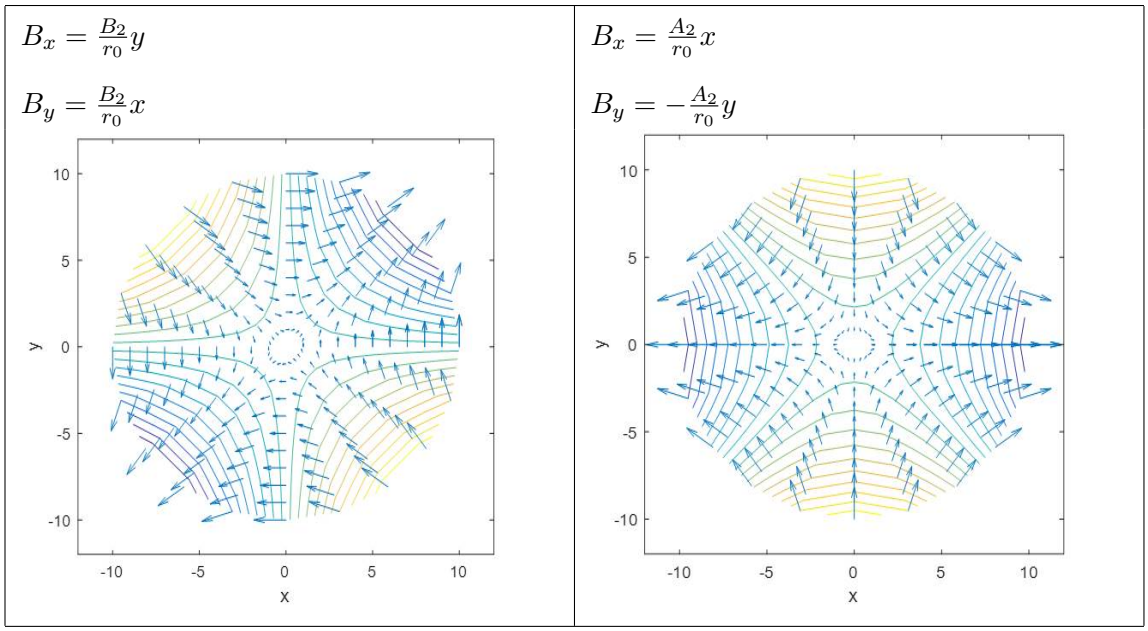

Figure 3.3: Field plot of upright quadrupole (left) and skew quadrupole (right)

For quadrupole field (n=3), we have

$$\begin{cases} B_r(r,\theta) = \left(\frac{r}{r_0}\right)[B_3 \sin 2\theta \ + A_3 \cos 2\theta] \\ B_\theta(r,\theta) = \left(\frac{r}{r_0}\right)[B_3 \cos 2\theta \ - A_3 \sin 2\theta] \end{cases} \tag{3.23}$$

or

$$\begin{cases} B_x(x,y) = \frac{1}{{r_0}^2}[B_3(2xy) + A_3(x^2 - y^2)] \\ B_x(x,y) = \frac{1}{{r_0}^2}[B_3\left(x^2 - y^2\right) - A_3(2xy)] \end{cases} \tag{3.24}$$

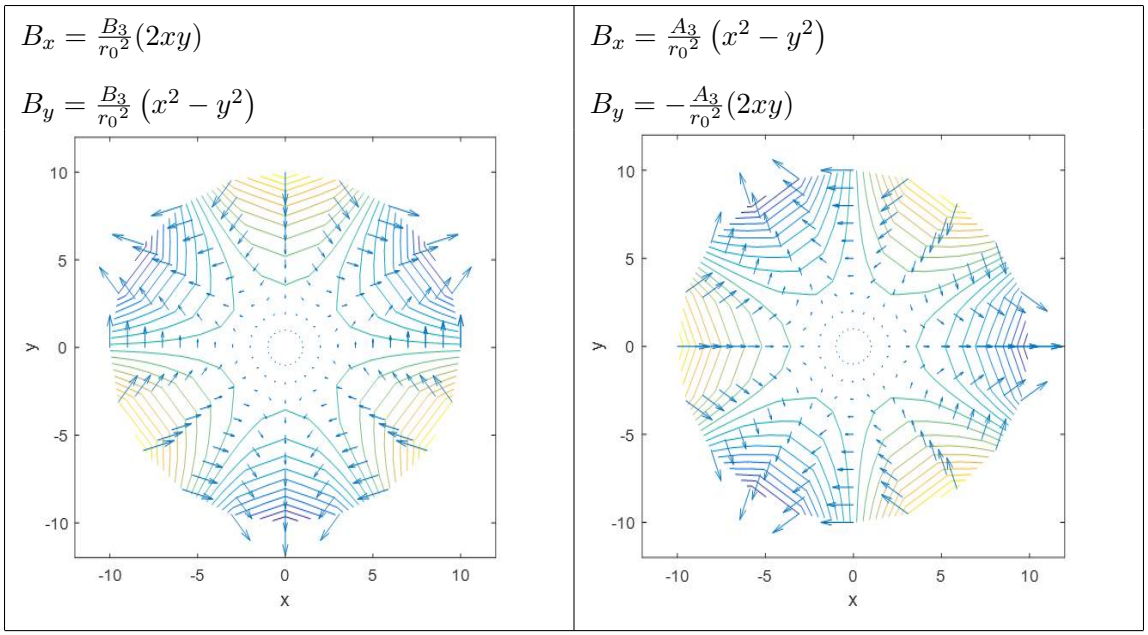

Figure 3.4: Field plot of upright sextupole (left) and skew sextupole (right)

One may notice that the Bn-only multipole field becomes An-only multipole field when it's rotated in CW by $\frac{\pi}{2n}$. The Bn-only field is called "normal" or "upright" field; the An-only field is called "skew" field. Define $C_n = \sqrt{{B_n}^2 + {A_n}^2}$ to be the magnitude of multipole coefficient and $\varphi_n = \text{atan}\left(\frac{A_n}{B_n}\right)$ to be the phase angle (also known as skew angle).

$$B_r(r,\theta) = \sum_{n=1}\left(\frac{r}{r_0}\right)^{n-1} C_n[\cos(\varphi_n)\sin(n\theta) \ + \sin(\varphi_n)\cos(n\theta)] \tag{3.25}$$

$$B_\theta(r,\theta) = \sum_{n=1}\left(\frac{r}{r_0}\right)^{n-1} C_n[\cos(\varphi_n)\cos(n\theta) \ - \sin(\varphi_n)\sin(n\theta)] \tag{3.26}$$

Simplifying it, we have the other form of multipole coefficient in terms of C_n and φ_n:

$$B_r(r,\theta) = \sum_{n=1}\left(\frac{r}{r_0}\right)^{n-1} C_n[\sin(n\theta + \varphi_n)\ ] \tag{3.27}$$

$$B_\theta(r,\theta) = \sum_{n=1}\left(\frac{r}{r_0}\right)^{n-1} C_n[\cos(n\theta + \varphi_n)\ ] \tag{3.28}$$

With these multipole coefficients, one can reconstruct the field as function of position and predict the interaction between magnetic field and charged particle beam.

3.2 FIELD DERIVATIVES

For beam dynamic or lattice design, the parameter of magnetic field is often the multipole strength, which is not necessary the multipole coefficients but the derivatives of field at origin. For dipole (n=1), the parameter of field is the field itself at origin (and anywhere else).

$$B_x(0,0) = \ A_1$$

$$B_y(0,0) = \ B_1$$

For quadrupole (n=2), the quadrupole strength (or gradient) is the first derivative at origin.

$$Grad\,(0,0) = \left[\frac{\partial B_y}{\partial x}\right]_{x=0;y=0} = \frac{B_2}{r_0}$$

$$Skew\ Grad\,(0,0) = \left[\frac{\partial B_x}{\partial x}\right]_{x=0;y=0} = \frac{A_2}{r_0}$$

For quadrupole (n=3), the sextupole strength (or sextupole gradient) is the second derivative at origin.

$$Sextupole\ Grad\,(0,0) = \left[\frac{\partial^2 B_y}{\partial x^2}\right]_{x=0;y=0} = \frac{2B_3}{{r_0}^2}$$

$$Skew\ Sextupole\ Grad\,(0,0) = \left[\frac{\partial^2 B_x}{\partial x^2}\right]_{x=0;y=0} = \frac{2A_3}{{r_0}^2}$$

In the general form, the relationship between derivative and multipole coefficient can be derived by:

$$\left[\frac{\partial^{n-1} B_\theta}{\partial r^{n-1}}\right] = \frac{\partial^{n-2}}{\partial r^{n-2}}\left\{\sum_{n=1}\frac{\partial}{\partial r}\left(\frac{r}{r_0}\right)^{n-1}\left[B_n\cos\left(n\theta\right)\ - A_n\sin(n\theta)\right]\right\}$$

$$= \frac{\partial^{n-2}}{\partial r^{n-2}}\left\{\sum_{n=2}\frac{(n-1)}{r_0}\left(\frac{r}{r_0}\right)^{n-2}\left[B_n\cos\left(n\theta\right)\ - A_n\ \sin(n\theta)\right]\right\}$$

$$= \frac{\partial^{n-3}}{\partial r^{n-3}}\left\{\sum_{n=3}\frac{(n-1)\,(n-2)}{{r_0}^2}\left(\frac{r}{r_0}\right)^{n-3}\left[B_n\cos\left(n\theta\right)\ - A_n\sin\left(n\theta\right)\ \right]\right\}$$

$$\overset{(at\ (n-1)^{th}\ derivative)}{\Longrightarrow}\left[\frac{\partial^{n-1} B_\theta}{\partial r^{n-1}}\right] = \sum_{n=n}\frac{(n-1)!}{{r_0}^{n-1}}\left(\frac{r}{r_0}\right)^{n-n}\left[B_n\cos\left(n\theta\right)\ - A_n\ \sin(n\theta)\right]$$

$$= \frac{(n-1)!}{{r_0}^{n-1}}[B_n \cos(n\theta) \ - A_n \sin(n\theta) \ ]$$

At origin the (n-1)th field derivative is:

$$\left[\frac{\partial^{n-1} B_y}{\partial x^{n-1}}\right]_{x=0;y=0} = \left[\frac{\partial^{n-1} B_\theta}{\partial r^{n-1}}\right]_{r=0;\theta=0} = \frac{(n-1)!}{{r_0}^{n-1}} B_n$$

Similarly, we can have

$$\left[\frac{\partial^{n-1} B_x}{\partial x^{n-1}}\right]_{x=0;y=0} = \left[\frac{\partial^{n-1} B_r}{\partial r^{n-1}}\right]_{r=0;\theta=0} = \frac{(n-1)!}{{r_0}^{n-1}} A_n$$

Reversing these equations, we get

$$\begin{aligned} B_n &= \frac{{r_0}^{n-1}}{(n-1)!}\left[\frac{\partial^{n-1} B_y}{\partial x^{n-1}}\right]_{x=0;y=0} \\ A_n &= \frac{{r_0}^{n-1}}{(n-1)!}\left[\frac{\partial^{n-1} B_x}{\partial x^{n-1}}\right]_{x=0;y=0} \end{aligned} \tag{3.29}$$

B_n and A_n can be acquired by performing polynomial fit on B vs x data from measurement. However, this approach assumes perfect azimuthal field symmetry, which is highly unrealistic due to all possible manufacture or assembling errors.

3.3 HARMONIC DECOMPOSITION

A more reliable and common way to acquire multipole coefficient from measurement is harmonic decomposition. In previous section, we know field components can be written as summation of cosine and sine functions multiplying with their B_n and A_n coefficients. We can pick up only the mth harmonic and null all other harmonics in the summation by using orthogonality of sinusoidal function.

$$\frac{1}{\pi}\int_{-\pi}^{\pi} cos(n\theta) \ cos(m\theta) d\theta = \begin{cases} 1, & n = m \\ 0, & n \neq m \end{cases}$$

$$\frac{1}{\pi}\int_{-\pi}^{\pi} sin(n\theta) \ sin(m\theta) d\theta = \begin{cases} 1, & n = m \\ 0, & n \neq m \end{cases}$$

$$\frac{1}{\pi}\int_{-\pi}^{\pi} sin\,(n\theta)\ cos(m\theta)d\theta = 0$$

Applying orthogonality between field component B_θ from Equation 3.16 and $cos(m\theta)$, the term b_m is picked up and all other terms are left zero.

$$LHS = \frac{1}{\pi}\int_{-\pi}^{\pi} B_\theta\,(r,\theta)\cos\,(m\theta)\ d\theta$$

$$RHS = \frac{1}{\pi}\int_{-\pi}^{\pi}\sum_{n=1}\left(\frac{r}{r_0}\right)^{n-1}[B_n\cos\,(n\theta)\ - A_n\sin(n\theta)]\cos(m\theta)d\theta$$

$$= \frac{1}{\pi}\int_{-\pi}^{\pi}\left(\frac{r}{r_0}\right)^{n-1} B_m\cos\,(m\theta)\ \cos\,(m\theta)\ + \sum_{n=1}\frac{1}{\pi}\int_{-\pi}^{\pi}(other\ terms)\cos(m\theta)\ d\theta$$

$$= \left(\frac{r}{r_0}\right)^{n-1} B_m\int_{-\pi}^{\pi}\cos\,(m\theta)\ \cos\,(m\theta)\ + \sum_{n=1} 0 = \left(\frac{r}{r_0}\right)^{n-1} B_m$$

If we acquire field data only at r=r_0 , we have:

$$B_m = \left[\frac{1}{\pi}\int_{-\pi}^{\pi} B_\theta\,(r_0,\theta)\cos(m\theta)d\theta\right]$$

Similarly, we can acquire A_m

$$A_m = -\left[\frac{1}{\pi}\int_{-\pi}^{\pi} B_\theta\,(r_0,\theta)\sin(m\theta)d\theta\right]$$

The relationship between individual multipole coefficient and field component becomes:

$$B_m = \frac{1}{\pi}\int_{-\pi}^{\pi} B_\theta\,(r_0,\theta)\cos\,(m\theta)\ d\theta = \frac{1}{\pi}\int_{-\pi}^{\pi} B_r\,(r_0,\theta)\sin(m\theta)d\theta \tag{3.30}$$

$$A_m = -\frac{1}{\pi}\int_{-\pi}^{\pi} B_\theta\,(r_0,\theta)\sin\,(m\theta)\ d\theta = \frac{1}{\pi}\int_{-\pi}^{\pi} B_r\,(r_0,\theta)\cos(m\theta)d\theta \tag{3.31}$$

In measurement, a complete and unbiased harmonic analysis requires the field vs position data of at least one circle, sampling with azimuthal symmetry.

3.4 FIELD QUALITY

The benefit of expressing the multipole coefficient of all order in the same unit is that they can be normalized to the primary multipole [11] [12]. The normalized multipole coefficients

are expressed as:

$$\begin{aligned} \overline{B}_n &= \frac{B_n}{C_p} * 10^4 \\ \overline{A}_n &= \frac{A_n}{C_p} * 10^4 \end{aligned} \tag{3.32}$$

A 10^4 multiplication factor is commonly used so 1 unit of $\overline{B}_n$and $\overline{A}_n$ is 0.01% of C_f, where C_f is the magnitude of the fundamental multipole coefficient.

3.5 ROTATING COIL

The analysis in previous section can be applied to any field vs position data collected by hall probe or stretch wires, but rotating coil method can sample with better efficiency and azimuthal symmetry. In this method, field data is measured indirectly by induction. Starting with Faraday's law:

$$V = -\frac{d\Phi}{dt}$$

the magnetic flux picked up by a single conductor loop is:

$$\Phi = \oint \overrightarrow{B} \bullet d\overrightarrow{A} = \oint \overrightarrow{B} \bullet \hat{n}\ dA$$

By intuition, we expand the magnetic field in cylindrical coordinate around the axis of rotation. The $\theta = 0$ plane can be referred to a static mechanical feature. For simplicity, it's chosen as horizontal plane. The two common coil geometries are radial and tangential. The former picks up only B_θ component and the latter picks up only B_r component.

3.5.1 RADIAL COIL

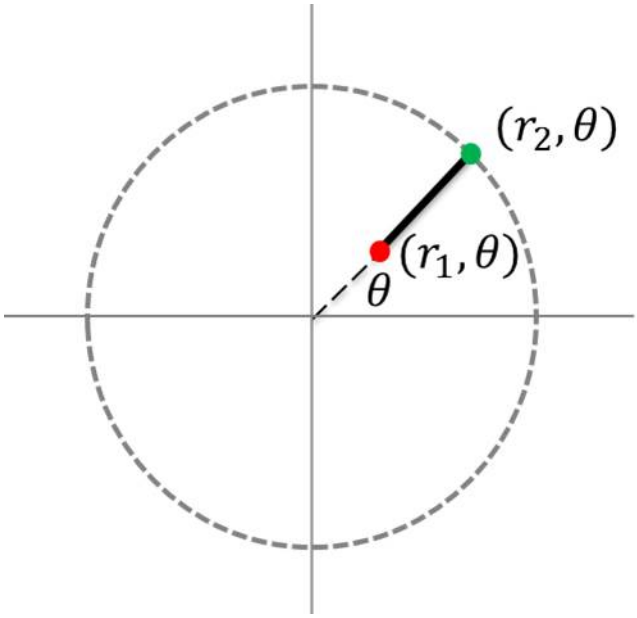

Figure 3.5: Axial view of radial coil

Since radial coil is always perpendicular to B_θ, flux of radial coil at angle θ is:

$$\Phi(\theta) = \oint B_\theta(\theta)\ dA$$

$$= \int_{r1}^{r2} \int B_\theta(\theta) dz dr$$

Define L as magnetic length such that $\int B_\theta dz = B_\theta L$, the function becomes

$$\Phi(\theta) = \int_{r1}^{r2} L \sum_{n=1} \left(\frac{r}{r_0}\right)^{n-1} [B_n \cos(n\theta)\ - A_n \sin(n\theta)] dr$$

$$= \sum_{n=1} \frac{Lr_0}{n} \left[\left(\frac{r_2}{r_0}\right)^n - \left(\frac{r_1}{r_0}\right)^n\right] [B_n \cos(n\theta)\ - A_n\ \sin(n\theta)]$$

$$= \sum_{n=1} K_n\ [B_n \cos(n\theta)\ - A_n \sin(n\theta)\ ]$$

$K_n = \frac{Lr_0}{n}\left[\left(\frac{r_2}{r_0}\right)^n - \left(\frac{r_1}{r_0}\right)^n\right]$ is known as the sensitivity factor, which only depends on coil geometry. When r_1=0 in radial coil, the returning conductor is on the axis of rotation and K_n becomes $\frac{Lr_0}{n}\left(\frac{r}{r_0}\right)^n$.

3.5.2 TANGENTIAL COIL

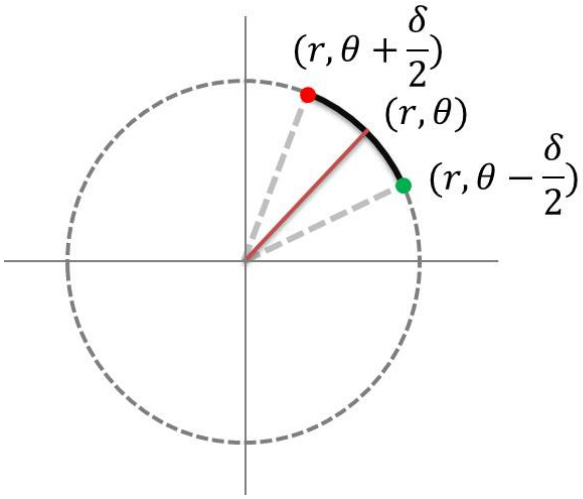

Figure 3.6: Axial view of tangential coil with opening angle δ

Similarly, tangential coil is always perpendicular to B_r, flux of tangential coil is:

$$\Phi(\theta) = \oint B_r \, dA$$

$$= \int_{\theta-\delta/2}^{\theta+\delta/2} \int B_r(\theta) dz \; r_0 d\varphi$$

$$= \int_{\theta-\delta/2}^{\theta+\delta/2} L \sum_{n=1} r \left(\frac{r}{r_0}\right)^{n-1} [B_n \sin(n\varphi) \; + A_n \cos(n\varphi)] d\varphi$$

$$= \sum_{n=1} \frac{Lr_0}{n} \left(\frac{r}{r_0}\right)^{n} [-B_n \cos(n\varphi) \; + A_n \sin(n\varphi)]|_{\theta-\delta/2}^{\theta+\delta/2}$$

Using trigonometry identity, the cosine and sine term become $-2\sin(n\theta)\sin\left(\frac{n\delta}{2}\right)$ and $2\cos(n\theta)\sin\left(\frac{n\delta}{2}\right)$, respectively.

Finally, we have: $\Phi = \sum_{n=1} \frac{2Lr_0}{n} \left(\frac{r}{r_0}\right)^{n} \sin\left(\frac{n\delta}{2}\right) [B_n \sin(n\theta) \; + A_n \cos(n\theta)]$

or

$$\Phi = \sum_{n=1} K_n [B_n \sin(n\theta) \; + A_n \cos(n\theta)]$$

where $K_n = \frac{2Lr_0}{n} \left(\frac{r}{r_0}\right)^{n} \sin\left(\frac{n\delta}{2}\right)$ is the sensitivity factor for tangential coil.

3.5.3 SINGLE WIRE AND GENERAL COIL FORM

When $\delta = \frac{\pi}{n}$ in tangential coil, K_n reaches maximum and is twice of K_n for single wire. Here we take quadrupole (n=2) as example. In figure 3.7 (left), tangent coil of $\frac{\pi}{2}$ open angle is exposed to magnetic flux of top right quadrant when it's at $\theta = \frac{\pi}{4}$. The figure 3.7 (right) shows four tangent coils with different path. They all have same flux exposure as long as the axial conductor segments are at the same location.

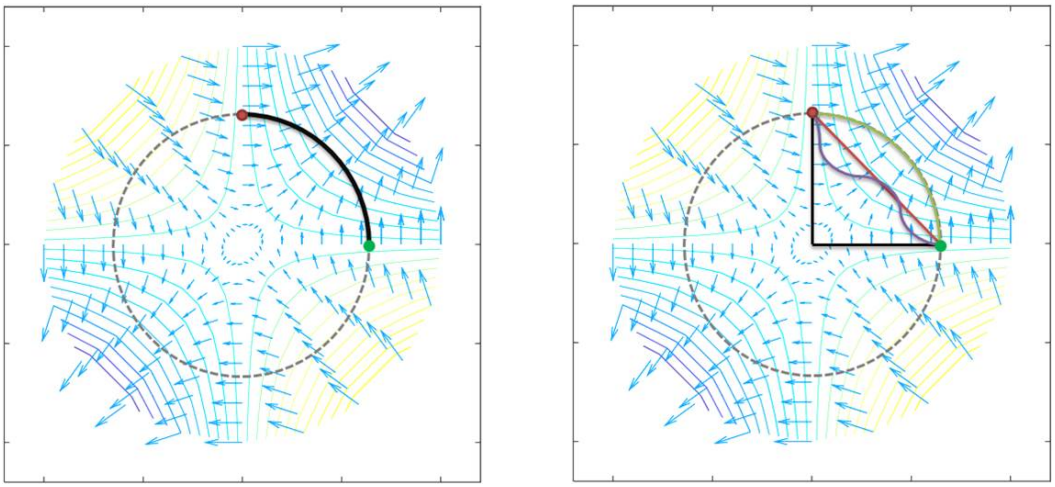

Figure 3.7: The $\frac{\pi}{2}$ tangential coil of "quarter-circle" geometry (left). The $\frac{\pi}{2}$ tangential coil when the vertex are connected by four different paths (right). All these coils have the same flux exposure.

The L-shape path's connection at origin can break into two segments. When a pair vertex (red) and vertex (green) node are added at origin, two radial coils are formed.

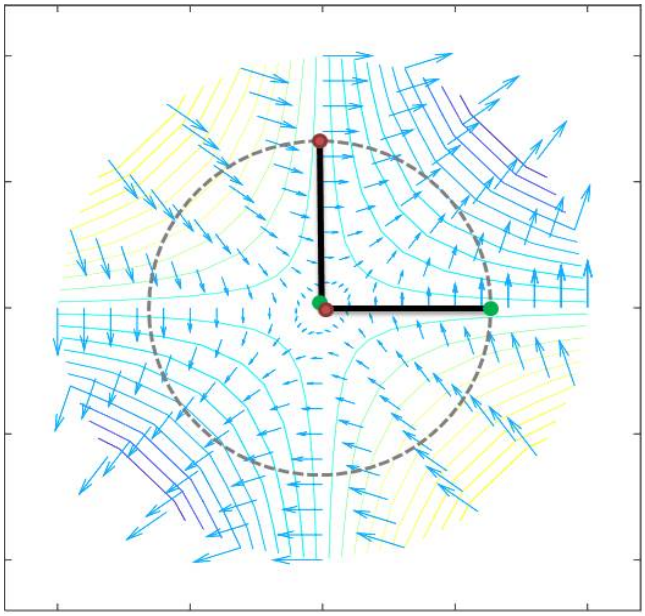

Figure 3.8: A pair of radial coil with opposite normal vector $+\widehat{\boldsymbol{\theta}}$ and $-\widehat{\boldsymbol{\theta}}$ are formed when L-shape $\frac{\boldsymbol{\pi}}{\mathbf{2}}$ tangential is disconnected at rotation axis.

Mathematically, the two configurations give identical result. At $\frac{\pi}{4}$ phase advance, the $\frac{\pi}{2}$ opening tangent loop measures flux:

$$\Phi = \sum_{n=1} \frac{2Lr_0}{n}\left(\frac{r}{r_0}\right)^n \sin\left(\frac{n\pi}{4}\right)\left[B_n \sin\left(n\theta + \frac{n\pi}{4}\right) + A_n \cos\left(n\theta + \frac{n\pi}{4}\right)\right]$$

For the two radial coils with opposite normal vector, the total flux is

$$\begin{aligned}\Phi = \sum_{n=1} \frac{Lr_0}{n}\left(\frac{r}{r_0}\right)^n &\left[B_n \cos(n\theta) - A_n \sin(n\theta)\right] \\ &+ (-1)\sum_{n=1} \frac{Lr_0}{n}\left(\frac{r}{r_0}\right)^n \left[B_n \cos\left(n\theta + \frac{n\pi}{2}\right) - A_n \sin\left(n\theta + \frac{n\pi}{2}\right)\right] \\ = \sum_{n=1} \frac{Lr_0}{n}\left(\frac{r}{r_0}\right)^n &\left[-B_n 2\sin\left(n\theta + \frac{n\pi}{4}\right)\sin\left(\frac{-n\pi}{4}\right) - A_n\, 2\cos\left(n\theta + \frac{n\pi}{4}\right)\sin\left(\frac{-n\pi}{4}\right)\right] \\ = \sum_{n=1} \frac{2Lr_0}{n}\left(\frac{r}{r_0}\right)^n &\sin\left(\frac{n\pi}{4}\right)\left[B_n \sin\left(n\theta + \frac{n\pi}{4}\right) + A_n \cos\left(n\theta + \frac{n\pi}{4}\right)\right]\end{aligned}$$

From previous example, we see that flux of single wire loop is only dependent of the axial conductor's transverse position and winding direction. For multiple loop combination, the flux can be expressed as summation of flux measured by each axial conductor

with proper sign. To make the derivation simpler, complex variable is introduced. First $B_n\cos(n\theta) - A_n\sin(n\theta)$ is rewritten as $Re\{[B_n + iA_n][\cos(n\theta) + i\sin(n\theta)]\}$ and it becomes $Re\left\{[B_n + iA_n]\, e^{in\theta}\right\}$. The flux picked up by single rotating wire at position angle $\theta + \alpha$ is:

$$\begin{aligned} & Re\left\{\frac{Lr_0}{n}\left(\frac{r}{r_0}\right)^n (B_n + iA_n)\, e^{in(\theta+\alpha)}\right\} \\ &= Re\left\{\frac{Lr_0}{n}\left(\frac{re^{i\alpha}}{r_0}\right)^n (B_n + iA_n)\, e^{in\theta}\right\} \\ &= Re\left\{K_n\,(B_n + iA_n)\, e^{in\theta}\right\} \end{aligned}$$

where the new sensitivity factor is $K_n = \frac{Lr_0}{n}\left(\frac{re^{i\alpha}}{r_0}\right)^n$. For coil constructed by multiple axial segments at different location with alternating winding direction, we get:

$$K_n = \sum_j^N \frac{Lr_0}{n}\left(\frac{r}{r_0}\right)^n e^{in\alpha_j}(-1)^j \tag{3.33}$$

This general form for flux of an arbitrary coil is [13]:

$$\Phi(\theta) = Re\left\{\sum_{n=1} K_n\,(B_n + iA_n)\, e^{in\theta}\right\} \tag{3.34}$$

3.5.4 MORGAN COIL

Morgen coil [14] [15] use special winding for particular harmonic order. For m^{th} order harmonic, "2m" axial-direction conductors are located equally spaced by $\frac{\pi}{m}$, with alternating winding direction. When n^{th} order harmonic is measured by m^{th} order Morgan coil, $\alpha_j = \left(\frac{j\pi}{m}\right)$. Therefore, $e^{in\left(\frac{j\pi}{m}\right)}(-1)^j = e^{i\pi j(1+\frac{n}{m})}$. This value is 1 when n = m, 3m, 5m, ... ,etc. Morgan coil is n times sensitive to its fundamental harmonic and the allowed harmonic with the peak $K_n = Lr_0\left(\frac{r}{r_0}\right)^n$. In these cases, flux measured by each wire is in phase. For other harmonic, the sensitivity is zero.

$$K_n = \frac{Lr_0}{n}\left(\frac{r}{r_0}\right)^n \sum_j^{2m} e^{i\pi j(1+\frac{n}{m})} = \begin{cases} \frac{Lr_0}{n}\left(\frac{r}{r_0}\right)^n * 2m, & n = m,\ 3m,\ 5m\ldots \\ 0, & n = else \end{cases}$$

Since each Morgan coil only measures its own fundamental harmonic, many of them are required to measure a magnet up to sufficient harmonic order. For dipole magnet, it may be reasonable to 5^{th} order. For quadrupole, it may be necessary to measure harmonic up to 10^{th} order. Space limit on winding fixture is the challenging especially for small aperture measurement. The angular position of each coil needs careful measurement with respect to the reference feature for $\theta = 0$ plane.

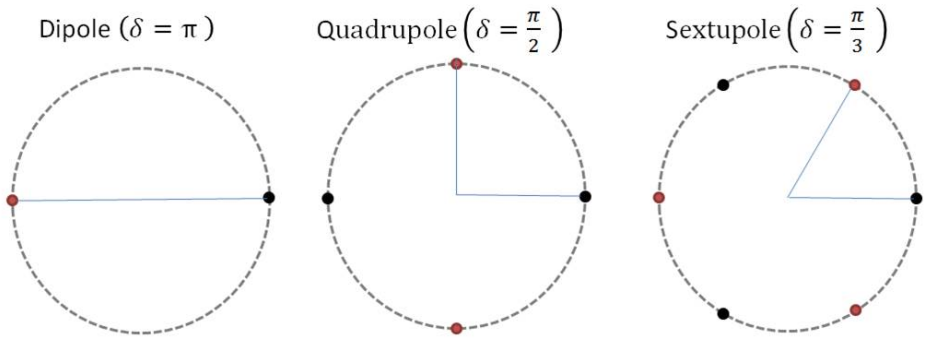

Figure 3.9: Morgan coil for first, second and third order harmonic. Black and red vertex represents conductor wound in opposite direction.

3.6 SIGNAL PROCESSING

The coil measures signal in voltage waveform:

$$V(t) = -\frac{d\Phi(\omega t)}{dt}$$

Since inconsistent rotation speed ω can affect signal strength, it's more common to analyze the signal after time integration.

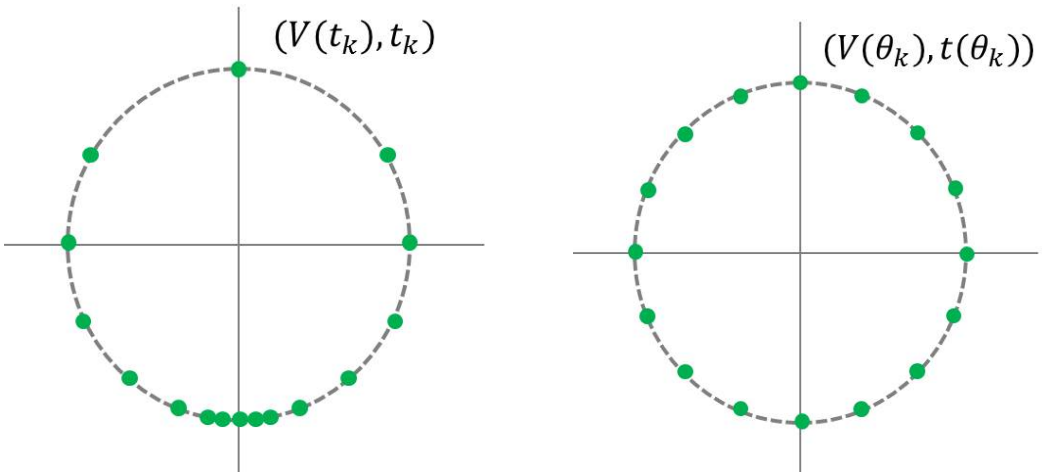

Figure 3.10: Asymmetric data per revolution caused by inconsistent rotation speed cause if sampling is time-based (left). Symmetric data collected when angle-based sampling is used (right).

During rotation, rotary encoder generates discrete signal when one unit of rotation $\delta\theta$ is executed. Then the integrator runs its build-in timer and stamp the time based on encoder signal. After integration, the discrete signal becomes

$$Vs\left[\theta_k\right] = \sum_{i=0}^{k} V\left[\theta_i\right] \delta t\left[\theta_i\right] = -\Phi[\theta_k] \tag{3.35}$$

$\theta_k = k\delta\theta$ is the angular position of coil. $V\left[\theta_i\right]$ is the voltage signal sampled at angular position θ_i. $\delta t\left[\theta_i\right]$is the lapse time between adjacent angular position. $N = \frac{2\pi}{\delta\theta}$ is the number of sampling point for one cycle. Applying Fast Fourier Transformation on both side of equation, we get:

$$\begin{aligned} FFT\left(Vs\right)_n &= -\sum_{n=1} K_n\left(B_n + iA_n\right) \sum_{k=1}^{N} e^{in\theta_k} e^{\frac{-i2\pi nk}{N_s}} \\ &= -\sum_{n=1} K_n\left(B_n + iA_n\right) \sum_{k=1}^{N} 1 \\ &= -N \sum_{n=1} K_n\left(B_n + iA_n\right) \end{aligned}$$

The harmonic coefficients in terms of integrated voltage signal are:

$$\begin{aligned} B_n &= -Re\left\{\frac{FFT\,(Vs)_n}{NK_n}\right\} \\ A_n &= -Im\left\{\frac{FFT\,(Vs)_n}{NK_n}\right\} \\ C_n &= \left|\frac{FFT\,(Vs)_n}{NK_n}\right| \\ \varphi_n &= atan\left(\frac{A_n}{B_n}\right) \end{aligned} \tag{3.36}$$

Where $FFT(Vs)[n]$ stands for the nth data of FFT signal. Notice that K_n is complex number written as:

$$K_n = \sum_j \frac{Lr_0}{n}\left(\frac{r}{r_0}\right)^n e^{in\alpha_j}(-1)^j$$

The sensitivity for the four coil types mention in previous section are presented here:

Radial coil:

$$K_n = \frac{Lr_0}{n}\left[\left(\frac{r_2}{r_0}\right)^n - \left(\frac{r_1}{r_0}\right)^n\right] \tag{3.37}$$

Tangential coil:

$$K_n = -i\frac{2Lr_0}{n}\left(\frac{r}{r_0}\right)^n \sin\left(\frac{n\delta}{2}\right) \tag{3.38}$$

Single wire:

$$K_n = \frac{Lr_0}{n}\left(\frac{r}{r_0}\right)^n \tag{3.39}$$

Morgan coil of mth harmonic:

$$K_n = \begin{cases} \frac{2mLr_0}{n}\left(\frac{r}{r_0}\right)^n, & n = m,\ 3m,\ 5m\ldots \\ 0, & n = else \end{cases} \tag{3.40}$$

3.7 ERROR PROPAGATION

The limiting factors of accuracy and precision in rotating coil method are dynamic position, signal resolution, and false signal. They are linked directly to data acquisition, data transmission noises, rotation speed consistency, and coil geometry.

$$C_n = \left|\frac{FFT\,(Vs)_n}{NK_n}\right|$$

$$\frac{\Delta C_n}{C_n} = \sqrt{\left(\frac{\Delta_{Voltage}}{C_n}\right)^2 + \left(\frac{\Delta_{time}}{C_n}\right)^2 + \left(\frac{\Delta_{\theta}}{C_n}\right)^2 + \left(\frac{\Delta_{K_n}}{C_n}\right)^2} \tag{3.41}$$

The first term depends on the ADC accuracy and the noise during data transmission. The second term depends on the time stamping process inside integrator. The third term depends on the rotation of coil in lab frame. The last term depends on the coil geometry and vibration in coil frame. If Voltage data is analyzed instead, the nth harmonic and error becomes:

$$C_n = \left|\frac{FFT\,(V)_n}{\omega N K_n}\right|$$

$$\frac{\Delta C_n}{C_n} = \sqrt{\left(\frac{\Delta_{Voltage}}{C_n}\right)^2 + \left(\frac{\Delta\omega}{\omega}\right)^2 + \left(\frac{\Delta_{\theta}}{C_n}\right)^2 + \left(\frac{\Delta_{K_n}}{C_n}\right)^2} \tag{3.42}$$

The only difference is that the error in integration time is replaced by error in rotation speed error.

3.7.1 ERROR AND NOISE IN DAQ AND DATA TRANSMISSION

There are three portion of error in voltage signal digitization: Gain error, offset error, and noise. The first two errors limit the accuracy and the last error limits the resolution and precision. The gain error and offset error are temperature dependent and can increase in time after each calibration. Therefore, it's important to operate the device in a temperature controlled environment and calibrate it in regular basis. The noise is often expressed in root mean square form. For high confidence, the peak to peak noise error use 3-sigma. The value of error and noise are also dependent to sampling rate and input scale. Noise in data transmission is different from digitizing noise. The source of this noise can be electrical noise from nearby hardware [15] (for example, power supply, computer, motors,..., etc.) and the signal carrier (slip ring, solder joint, and cable). This type of noise has specific frequency that can be dependent to the measurement. For example, slip ring noise is coupled with rotation. The noise from function generator in pulse magnet is directly related

to measurement too. The expression for systematic voltage signal error is:

$$\Delta V_{gain} + \ \Delta V_{offset} + \Delta V_{system\ noise}$$

$$= V_{in}[\theta_i] * gain\ error + \ \Delta V_{offset} + \Delta V_{system\ noise}[\theta_i]$$

The offset error has no contribution after FFT. However, if signal strength is close to measurement range of DAQ, this offset error may cause signal loss when overloaded signal gets truncated. The third part of error is noise from environment and signal carrier. The noise from DAQ is excluded in this calculation for systematic error because it's random noise. The error contribution due to voltage signal error is derived as:

$$\frac{\Delta_{Voltage}}{C_n} = \frac{1}{FFT\left(Vs\right)_n} FFT\left\{\sum_{i=0}^{k}\left(V_{in}[\theta_i] * gain\ error + \Delta V_{system\ noise}[\theta_i]\right)\delta t[\theta_i]\right\}$$

$$= gain\ error + \frac{FFT(\Delta V_{system\ noise})_n * Rotation\ period}{FFT\left(Vs\right)_n} \tag{3.43}$$

The gain error can be found in DAQ specification. The spectrum of system noise needs to be evaluated by background measurement.

The resolution of voltage signal depends on signal to noise ratio. For a resolvable signal, the SNR need to be at least greater than two. Therefore the minimum voltage signal of nth harmonic is:

$$FFT\left(V\right)_n \geq N * 2 * (3\sigma_V)$$

,where σ_V is the noise of DAQ. Notice that FFT magnifies the result by N times. This N factor needs to be compensated before comparing it with time-domain magnitude. The minimum resolvable harmonic strength becomes:

$$\min(|C_n|) = \left|\frac{2 * (3\sigma_V)}{\omega K_n}\right|$$

,where ω is the average rotation speed.

For example, if $\sigma_V = 1uV$, $\omega = 1Hz$, and $K_6 = 0.2$, the minimum resolvable 6^{th} harmonic $|C_6|$ would be ~5 uT. If the fundamental harmonic, say quadrupole, is 0.05T, the ratio

between 6^{th} and 2^{nd} harmonic is 1 unit or 100 ppm. This is measurement precision for 6^{th} harmonic by DAQ, assuming all other noises are zero. When evaluating the final precision of system, all source of noise will contribution to the numerator.

The error in voltage signal caused by inconsistent rotation speed is discussed in next section because it's an error due to dynamic error.

3.7.2 ERROR AND NOISE IN INTEGRATION TIME

There are two errors in signal involves with time. The first error is due to inconsistent rotation speed. The effect to voltage signal strength can be removed by time integration. If integration happens after digitization, there will be numerical integration error. For periodic function, trapezoidal method has really high accuracy for small numbers of point per harmonic cycle [16]. The second error comes from the minimum step and accuracy in DAQ timer. Because digital trigger is used, the time accuracy of voltage signal can only be as good as the trigger pulse width. The error contribution of error in time is:

$$\frac{\Delta_{time}}{C_n} = \frac{1}{FFT\,(Vs)_n} FFT\left\{\sum_i^k V[\theta_i]\ \Delta t_{trigger}\ \right\}$$

$$= \frac{1}{FFT\,(Vs)_n} FFT\left\{\sum_i^k V[\theta_i] * \delta t[\theta_i]\right\}\ \frac{\Delta t_{trigger}}{\delta t[\theta_i]} \approx \frac{\Delta t_{trigger}}{T/N} \tag{3.44}$$

Notice that time error $\Delta t_{trigger}$ is additional to correct time interval $\delta t[\theta_i]$. Since rotation speed is not constant, $\sum_k^{N_s} V[\theta_i]$ need to multiply with proper $\delta t[\theta_i]$ to be zero. The residual signal due to $\Delta t_{trigger}$ will be observed as vertical drift on voltage-time signal. T/N is the rotation period divided by number of encoder pulses. The other possible error happens when the encoder signal is miss-counted. The consequence is a discontinuity on voltage-time signal. As we know, discontinuity in signal generates combination of infinite Fourier series. It will generate a broad band error spectrum to the result signal. Test on encoder counts needs to be performed on regular basis. If miscounting occurs consistently, the

encoder should be replaced. There's also time error due current sweep time in AC or pulse magnet but it is not discussed in this thesis.

3.7.3 ERROR IN ANGULAR POSITION

The error caused by systematic error $\Delta\theta$ is simply an angular shift in integrated signal:

$$\frac{\Delta_\theta}{C_n} = \frac{1}{FFT\,(Vs)_n} FFT\left[\sum_j^k V[\theta_j]\delta t[\theta_j] e^{in\Delta\theta}\right] = e^{in\Delta\theta} \tag{3.45}$$

This $\Delta\theta$ error exists due to minimum step of δt in time integral. The angular misplacement of coil is not discussed here but in coil geometry section. When $V\,[\theta_i]\,\delta t\,[\theta_i]$ is calculated, it actually represents the average flux portion $\delta\,\Phi$ at $\theta_k + \frac{\delta\theta}{2}$ position, regardless of integration method. Therefore the analysis result will be skewed by $\frac{\delta\theta}{2}$ in the direction of rotation. This error can be reduced by having a higher step resolution encoder. Alternatively, it can be easily removed by performing a measurement in reversed direction and take the average.

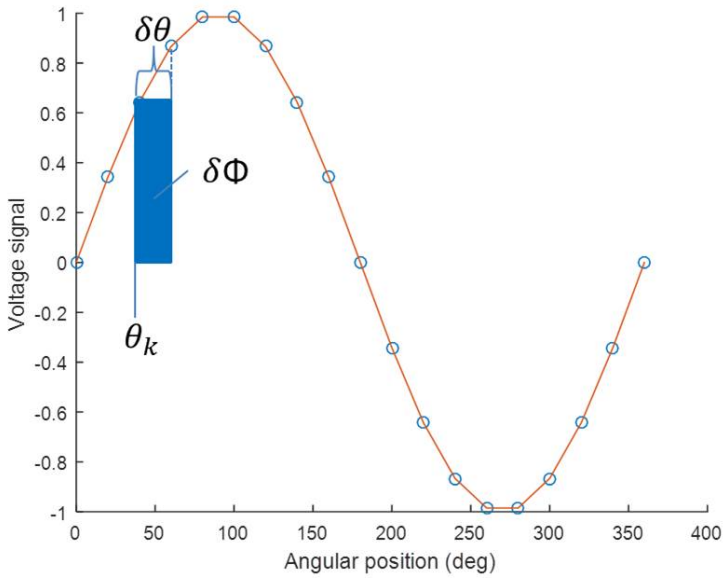

Figure 3.11: Integration fragment $\boldsymbol{V\,[\theta_i]\,\delta t\,[\theta_i]}$ doesn't give $\boldsymbol{\delta\,\Phi\,[\theta_i]}$ but $\boldsymbol{\delta\,\Phi\left[\theta_i + \frac{\delta\theta}{2}\right]}$

3.7.4 ERROR IN COIL GEOMETRY

The general form for sensitivity of single wire is:

$$K_n = \frac{Lr_0}{n}\left(\frac{r}{r_0}\right)^n e^{in\alpha}$$

Both r and α has systematic error $\Delta r,\ \Delta\alpha$ and random error σ_r , σ_α along z direction.

RADIAL POSITION ERROR

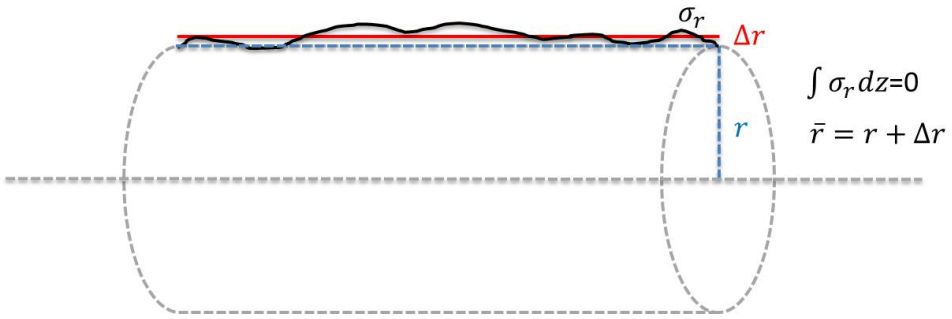

Figure 3.12: Systematic and random error in radial position of single conductor segment.

For systematic error in radial position, we Taylor expand K_n at r. Because integration $\int \sigma_r\ dz$ along conductor segment has to be zero, the random error cannot contribute to first order error.

$$\begin{aligned} K_n\left(r + \Delta r + \sigma_r\right) &= K_n\left(r\right) + \left.\frac{\partial K_n}{\partial r}\right|_r * \left(r + \Delta r + \sigma_r - r\right) + \ldots \\ &= K_n + \frac{nK_n}{r}\Delta r \\ &= K_n\left(1 + n\frac{\Delta r}{r}\right) \end{aligned}$$

or

$$\frac{\Delta_{r,syst}}{K_n} = n\frac{\Delta r}{r}. \tag{3.46}$$

This error often comes from winding fixture size error or placement error of fixture with respect to rotational axis. For radial coil, the conductor is often wounded on a fixture first. The fixture is then mounted on a shaft with some kind of positioning feature. These errors

in size and position accumulate. Also, the shaft is connected to motor with possible (but often small) concentricity error. The printed circuit board (PCB) coil would have more concentricity error if cylindrical shaft is not used. For simplicity, error in angular position is assumed perfect in this section. In coil design, the total error caused by radial position can be calculated by summing up all the geometric freedom with associated manufacture tolerance:

$$\sum_{degree\ of\ freedom} n\frac{\Delta r}{r}$$

The systematic error can be eliminated by calibration using know magnetic field source. It can be a magnetic standard or a dipole that's characterized by NMR probe. The calibration process updates the radial position to $\overline{r} = r + \Delta r$ so the random error is compensated.

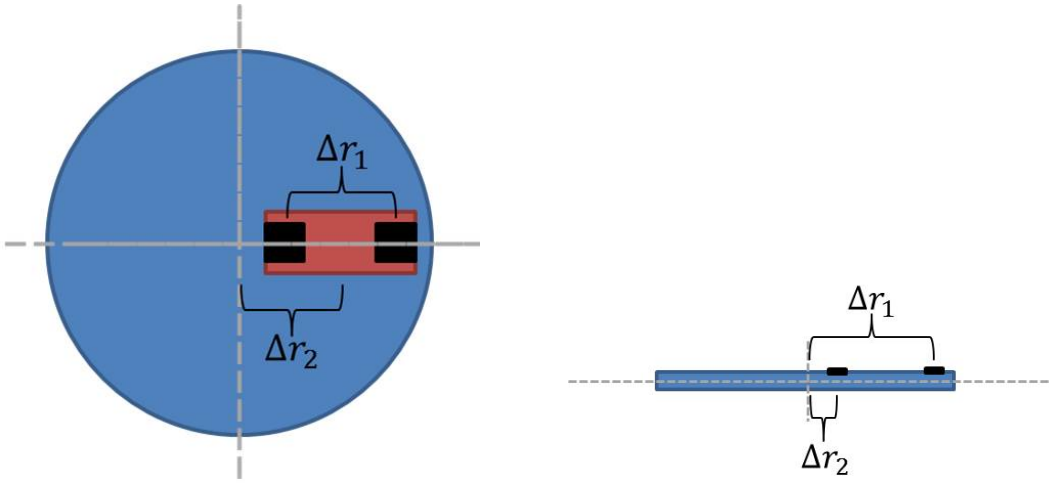

Figure 3.13: Radial position errors in traditional radial coil (Left) and in PCB coil (Right)

For random error in radial position, we Taylor expand K_n at $\overline{r} = r + \Delta r$ (i.e. averaged radius of conductor):

$$\begin{aligned} K_n\left(\overline{r} + \sigma_r\right) &= K_n\left(\overline{r}\right) + \left.\frac{\partial K_n}{\partial \overline{r}}\right|_{\overline{r}} * \left(\overline{r} + \sigma_r - \overline{r}\right) + \frac{1}{2}\left.\frac{\partial^2 K_n}{\partial \overline{r}^2}\right|_{\overline{r}} * \left(\overline{r} + \sigma_r - \overline{r}\right)^2 + \ldots \\ &= K_n + \frac{n(n-1)K_n}{2\overline{r}^2}{\sigma_r}^2 \\ &= K_n\left(1 + \frac{n(n-1)}{2}\left(\frac{\sigma_r}{\overline{r}}\right)^2\right) \end{aligned}$$

or

$$\frac{\Delta_{r,rand}}{K_n} = \frac{n(n-1)}{2}\left(\frac{\sigma_r}{\bar{r}}\right)^2 \tag{3.47}$$

A random error in coil cannot be calibrated but it will attenuated by adding more conductor segments. Since the segments are electrically connected, the random error spread over the prolonged conductor length. A coil of "N" axial segments of conductor should have its random error drop by factor of $\frac{1}{N}$.

ANGULAR POSITION ERROR

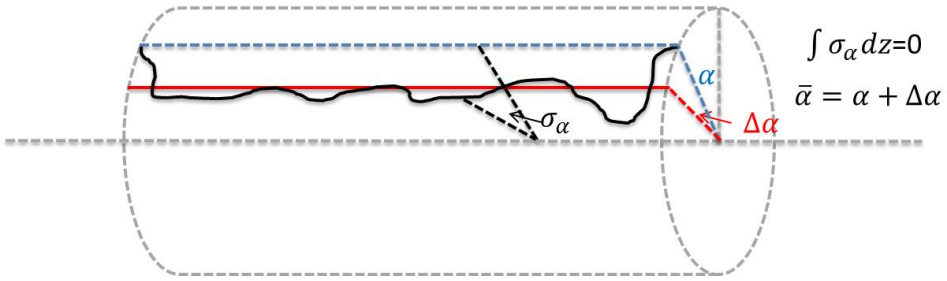

Figure 3.14: Systematic and random error in angular position of single conductor segment.

Similarly, for systematic error in angular position, we Taylor expand K_n at α:

$$K_n(\alpha + \Delta\alpha + \sigma_\alpha) = K_n + \left.\frac{\partial K_n}{\partial \alpha}\right|_\alpha * (\alpha + \Delta\alpha + \sigma_\alpha - \alpha) + \ldots$$

$$= K_n + inK_n\Delta\alpha$$

$$= K_n(1 + in\Delta\alpha)$$

or

$$\frac{\Delta_{\alpha,syst}}{K_n} = in\Delta\alpha \tag{3.48}$$

Notice that this error is imaginary so in addition to error in magnitude, it also gives error in skew angle. The systematic angular error is equivalent to an angular offset with respect to zero reference. It can be calibrated by a known magnetic field source with known skew

angle with respect to the angular reference. Alternatively, we can performed a measurement reversely and take the average of two measurement data.

Particularly, angular position error is the major manufacture error in tangential coil. The conductor often wound directly on the rotating shaft. It eliminates one source of error in assembling. The shaft is machined with notches to accommodate conductors. In this way, the error in radial position should be well-controlled by natural unless shaft and motor has concentricity issue. Recall that sensitivity for tangential coil is:

$$K_n = -i\frac{2Lr_0}{n}\left(\frac{r}{r_0}\right)^n \sin\left(\frac{n\delta}{2}\right)$$

When two conductor segments have systematic error $\Delta\alpha_1$and $\Delta\alpha_2$, the systematic error in opening angle becomes $\Delta\delta = |\Delta\alpha_1 - \Delta\alpha_2|$. Taylor expand K_n at δ gives

$$\begin{aligned} K_n\left(\delta + \ \Delta\delta + \sigma_\delta\right) &= K_n + \left.\frac{\partial K_n}{\partial\delta}\right|_\delta * \left(\delta + \Delta\delta + \sigma_\delta - \delta\right) + \ldots \\ &= K_n + K_n\left(\frac{n}{2}\right) cos\left(\frac{n\delta}{2}\right)\Delta\delta \\ &= K_n\left[1 + \left(\frac{n}{2}\right) cos\left(\frac{n\delta}{2}\right)\Delta\delta\right] \end{aligned}$$

or

$$\frac{\Delta_{\delta,syst}}{K_n} = \left(\frac{n}{2}\right) cos\left(\frac{n\delta}{2}\right)\Delta\delta \tag{3.49}$$

The systematic error in angular position for tangential coil is the same as single wire case, with substitution of $\Delta\alpha = \frac{\Delta\alpha_1 + \Delta\alpha_2}{2}$.

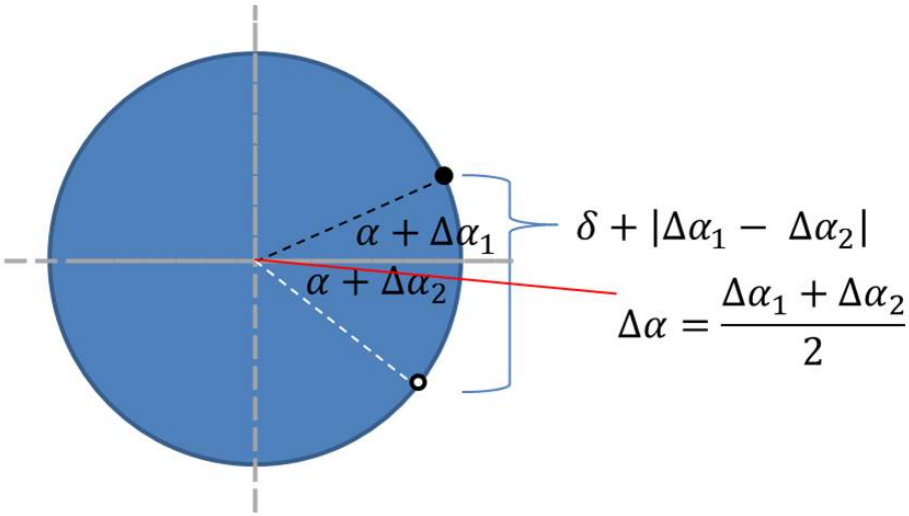

Figure 3.15: Angualr position errors in tangential coil

For random error in angular position, we Taylor expand K_n at $\overline{\alpha} = \alpha + \Delta\alpha$ (i.e. averaged angle of conductor):

$$\begin{aligned} K_n\left(\overline{\alpha} + \sigma_\alpha\right) &= K_n + \left.\frac{\partial K_n}{\partial \overline{\alpha}}\right|_{\overline{\alpha}} * \left(\overline{\alpha} + \sigma_\alpha - \overline{\alpha}\right) + \frac{1}{2}\left.\frac{\partial^2 K_n}{\partial \overline{\alpha}^2}\right|_{\overline{\alpha}} * \left(\overline{\alpha} + \sigma_\alpha - \overline{\alpha}\right)^2 + \ldots \\ &= K_n - \frac{n^2 K_n {\sigma_\alpha}^2}{2} \\ &= K_n\left(1 - \frac{n^2}{2}{\sigma_\alpha}^2\right) \end{aligned}$$

or

$$\frac{\Delta_{\alpha,rand}}{K_n} = -\frac{n^2}{2}{\sigma_\alpha}^2 \tag{3.50}$$

In the case of tangential coil, the random error is derived by simply substituting σ_α by $\frac{\sigma_\alpha}{2}$ because the length of axial conductor segment is doubled. Therefore we get

$$\frac{\Delta_{\delta,rand}}{K_n} = -\frac{n^2}{8}{\sigma_\alpha}^2 \tag{3.51}$$

For coil of N axial conductor segments, the general form of sensitivity error due to positional error can be calculated by:

$$|\Delta K_n| = \sqrt{\left(\sum_j^N \Delta_{r_j,syst}\right)^2 + \left(\sum_j^N \Delta_{\alpha_j,syst}\right)^2 + \left(\frac{\Delta_{r_j,rand}}{N}\right)^2 + \left(\frac{\Delta_{\alpha_j,rand}}{N}\right)^2}$$

The error in harmonic content due to sensitivity error is acquired:

$$\frac{\Delta_{Kn}}{C_n} = \sqrt{\left(\sum_j^N \frac{\Delta_{r_j,syst}}{K_n}\right)^2 + \left(\sum_j^N \frac{\Delta_{\alpha_j,syst}}{K_n}\right)^2 + \left(\frac{\Delta_{r_j,rand}}{NK_n}\right)^2 + \left(\frac{\Delta_{\alpha_j,rand}}{NK_n}\right)^2} \quad (3.52)$$

This formula assumes that errors in radial and angular position are independent. There are cases when the two error couples. For example, the radial or tangential coil can tilt with respect to its center of mass. The other example would be the occasion when the shaft is not concentric to motor axis. Discussion of these special cases can be found in other paper [17].

3.7.5 COIL VIBRATION

While rotation speed error is removed from the formula of signal strength after time integration, the vibration triggered by time varying angular velocity can cause fake signal, especially when the speed varies periodically. With proper choice of rotation speed, hundreds of measurement can be collected within a minutes. The random vibrational error soon vanishes. The only observable vibrations are systematic and have to be periodic. Although the vibration can be detected by sensor and measured for frequency, it cannot be eliminated by calibration.

TRANSVERSE VIBRATION

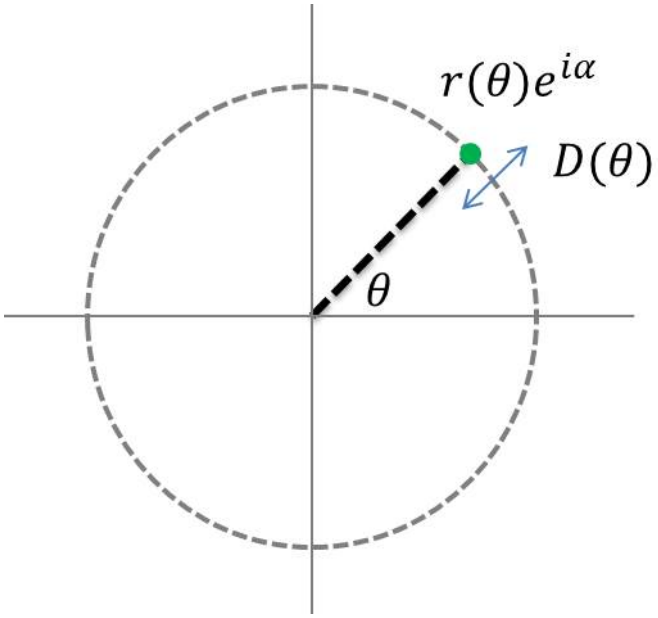

Figure 3.16: Transverse vibration of displacement D

We know flux of nth order harmonic for single rotating wire at θ is written as:

$$\Phi_n(\theta) = Re\left\{[B_n + iA_n]\, K_n e^{in\theta}\right\}$$

with

$$K_n = \frac{Lr_0}{n}\left(\frac{re^{i\alpha}}{r_0}\right)^n$$

When Transverse vibration happens at angular position θ, position of wire moves by $D(\theta)$ and pickup field at wrong position. Therefore we have:

$$\Phi_n(\theta)_{Trans.\ \ vib.} = Re\left\{\frac{Lr_0}{n}\left(\frac{re^{i\alpha} + D(\theta)}{r_0}\right)^n [B_n + iA_n]\, e^{in\theta}\right\}$$

Transverse vibration is a radial displacement function that has periodicity of θ. Therefore we can express it as Fourier series:

$$D(\theta) = \sum_{p=-\infty}^{\infty} D_p e^{ip\theta}$$

Before deriving for general form, we need to verify if the expression is valid for trivial cases. When wire is sensing dipole field, transverse vibration should have no effect on flux measurement due to dipole field's uniformity. Mathematically, it means

$$\Phi_1(\theta)_D = Re\left\{\frac{Lr_0}{1}\left(\frac{re^{i\alpha}+D(\theta)}{r_0}\right)^1[B_1+iA_1]e^{i\theta}\right\} = Re\left\{\frac{Lr_0}{1}\left(\frac{re^{i\alpha}}{r_0}\right)^1[B_1+iA_1]e^{i\theta}\right\}$$

To satisfy this condition, $\frac{D(\theta)}{r_0}e^{i\theta}$ has to be zero all the time, we redefine the vibration as [17]:

$$D(\theta) = \sum_{p=-\infty}^{\infty} D_p e^{i(p-1)\theta}$$

The derivation becomes:

$$\Phi_n(\theta)_D = Re\left\{\frac{Lr_0}{n}\left(\frac{re^{i\alpha}+D(\theta)}{r_0}\right)^n[B_n+iA_n]e^{in\theta}\right\}$$

$$= Re\left\{\frac{Lr_0}{n}\left[\left(\frac{re^{i\alpha}}{r_0}\right)^n + n\left(\frac{re^{i\alpha}}{r_0}\right)^{n-1}\left(\frac{D(\theta)}{r_0}\right)+\dots\right][B_n+iA_n]e^{in\theta}\right\}$$

$$\approx Re\left\{\frac{Lr_0}{n}\left[\left(\frac{re^{i\alpha}}{r_0}\right)^n + n\frac{n-1}{n-1}\left(\frac{re^{i\alpha}}{r_0}\right)^{n-1}\left(\frac{D(\theta)}{r_0}\right)\right][B_n+iA_n]e^{in\theta}\right\}$$

$$= Re\left\{K_n[B_n+iA_n]e^{in\theta} + (n-1)K_{n-1}\left(\frac{D(\theta)}{r_0}\right)[B_n+iA_n]e^{in\theta}\right\}$$

In the end, we get

$$\Phi_n(\theta)_D \approx \Phi_n(\theta) + Re\left\{(n-1)K_{n-1}\left(\frac{D(\theta)}{r_0}\right)[B_n+iA_n]e^{in\theta}\right\}$$

The first them is the non-perturbed nth flux. The second term is the erroneous flux $\Delta\Phi$ due to transverse vibration. Substituting $D(\theta) = \sum_{-\infty}^{\infty} D_p e^{i(p-1)\theta}$ into it, we have

$$\Delta\Phi = Re\left\{(n-1)K_{n-1}\left(\frac{\sum_{-\infty}^{\infty} D_p e^{i(p-1)\theta}}{r_0}\right)[B_n+iA_n]e^{in\theta}\right\}$$

$$= Re\left\{(n-1)K_{n-1}[B_n+iA_n]\sum_{-\infty}^{\infty}\frac{D_p}{r_0}e^{i(p+n-1)\theta}\right\}$$

After FFT, the term with $e^{i(p+n-1)\theta}$ multiplier will be "deciphered" as the (p+n-1)th harmonic Φ_{p+n-1}. Therefore we have:

$$Re\left\{(n-1)K_{n-1}[B_n+iA_n]\frac{D_p}{r_0}e^{i(p+n-1)\theta}\right\} = \Phi_{p+n-1}$$

$$= Re\left\{\left[B_{p+n-1} + iA_{p+n-1}\right] K_{p+n-1} e^{i(p+n-1)\theta}\right\}$$

Equating real and imaginary part, we get the following expressions for erroneous harmonic for (p+n-1)th order harmonic reading due to nth order harmonic field and transverse vibration of $e^{i(p-1)\theta}$periodicity. For simplicity, $p + n - 1$ is replaced by m. After changing these indices, we acquire the form for transverse vibration error for mth harmonic [17].

$$\Delta B_m = (n-1)\left(\frac{K_{n-1}}{K_m}\right)\left(\frac{D_{m-n+1}}{r_0}\right) B_n$$

$$\Delta A_m = (n-1)\left(\frac{K_{n-1}}{K_m}\right)\left(\frac{D_{m-n+1}}{r_0}\right) A_n$$

$$\frac{\Delta C_m}{C_n} = (n-1)\left(\frac{K_{n-1}}{K_m}\right)\left(\frac{D_{m-n+1}}{r_0}\right) \tag{3.53}$$

For example, if quadrupole (n=2) is under test and vibration of displacement D=0.001*r$_0$ occurs at frequency 2 rps (p=2), the sextupole harmonic (2+2-1=3) will have an extra reading:

$$\frac{\Delta C_3}{C_2} = \left(\frac{K_1}{K_3}\right) 0.001$$

Usually K_1/ K_3 is larger than 1. The fake result of more than 10unit presents and there's no legit way to distinguish it from actual sextupole content.

TORSIONAL VIBRATION

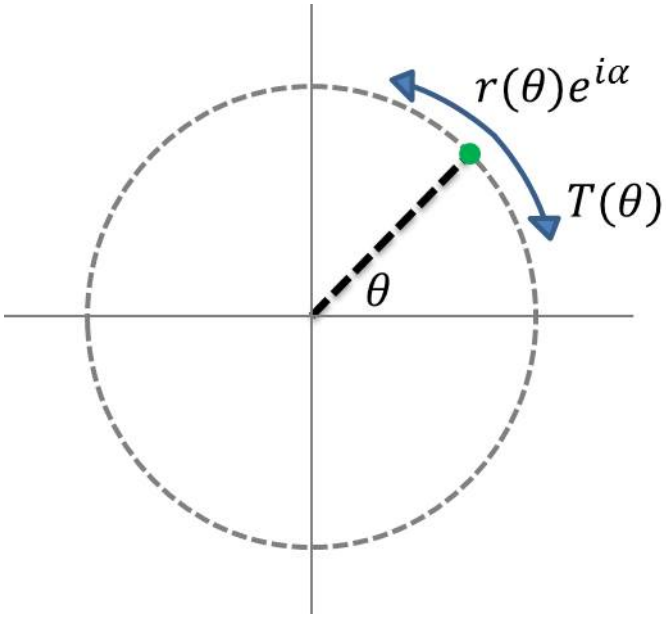

Figure 3.17: Torsional vibration of angular displacement T

Torsional vibration is an angular displacement function that has periodicity of θ. Again, using Fourier series, we have

$$T(\theta) = \sum_{\mathrm{p}=-\infty}^{\infty} T_p e^{ip\theta}$$

Applying $T(\theta)$ term to sensitivity of single rotating wire, the n^{th} order flux can be expressed as:

$$\Phi_n(\theta)_T = Re\left\{\frac{Lr_0}{n}\left(\frac{re^{i\alpha+iT(\theta)}}{r_0}\right)^n [B_n + iA_n]\, e^{in\theta}\right\}$$

$$= Re\left\{\frac{Lr_0}{n}\left(\frac{re^{i\alpha}}{r_0}\right)^n [B_n + iA_n]\, e^{in(\theta+T(\theta))}\right\}$$

$$= Re\left\{K_n [B_n + iA_n]\, [e^{in\theta} + inT(\theta)e^{inT(\theta)} + \dots\right\}$$

$$\approx Re\left\{K_n [B_n + iA_n]\, e^{in\theta} + inK_n T(\theta)\, [B_n + iA_n]\, e^{in\theta}\right\}$$

$$\Phi_n(\theta)_T \approx \Phi_n(\theta) + Re\left\{inK_n T(\theta)\, [B_n + iA_n]\, e^{in\theta}\right\}$$

The second term is the erroneous flux signal due to torsional vibration.

Substituting $T(\theta) = \sum_{-\infty}^{\infty} T_p e^{ip\theta}$ into it, we have

$$\Delta\Phi = Re\left\{inK_n \sum_{p=-\infty}^{\infty} T_p e^{ip\theta}\left[B_n + iA_n\right] e^{in\theta}\right\} = Re\left\{inK_n\left[B_n + iA_n\right] \sum_{p=-\infty}^{\infty} T_p e^{i(p+n)\theta}\right\}$$

After FFT, this erroneous signal due to n^{th} order field harmonic and torsional vibration of $e^{ip\theta}$ will be "deciphered" as the $(p+n)^{th}$ order harmonic:

$$Re\left\{inK_n\left[B_n + iA_n\right] T_p e^{i(p+n)\theta}\right\} = \Phi_{p+n}(\theta) = Re\left\{K_{p+n}\left[B_{p+n} + iA_{p+n}\right] e^{i(p+n)\theta}\right\}$$

Again, replace $p + n - 1$ by m, we have [17]:

$$\begin{aligned}
\Delta B_m &= -n\left(\frac{K_n}{K_m}\right) T_{m-n} A_n \\
\Delta A_m &= n\left(\frac{K_n}{K_m}\right) T_{m-n} B_n \\
\frac{\Delta C_m}{C_n} &= n\left(\frac{K_n}{K_m}\right) T_{m-n}
\end{aligned} \tag{3.54}$$

In quadrupole example (n=2), if 1 mrad angular shift occurs at frequency of 2 rps (p=2), The octupole harmonic will have an additional reading:

$$\frac{\Delta C_4}{C_2} = 2\left(\frac{K_2}{K_4}\right) 0.001$$

Usually, K_2/k_4 is larger than 1. The octupole content has extra 20unit of fake result concluded in measurement report.

3.7.6 COMPENSATION (BUCKING COIL)

Even with this coupling relationship between source harmonic and target harmonic known, it's not practical to measure these D_p and T_p values for error compensation. A practical way to reject these errors is by nulling the sensitivity K_{n-1} and K_n of the source harmonic using bucking coil(s). When vibrational error is picked up by main coil, the same amount of error is picked up by the bucking coil(s) so such error is canceled out in the summation signal. The summation can happen before or after digitizing. For analog bucking, main

coil and bucking coil signal are electrically connected so the vibrational error, along with the fundamental harmonic, is removed before digitizing. For magnet with field quality requirement, the strength of erroneous harmonics are usually 10^{-4} smaller in magnitude relative to fundamental harmonic. In this way, the signal can be digitized with larger gain ratio and have better resolution. The drawback is that the coil geometry and turn ratios of main coil and bucking coils needs to workout exactly for zero net sensitivity.

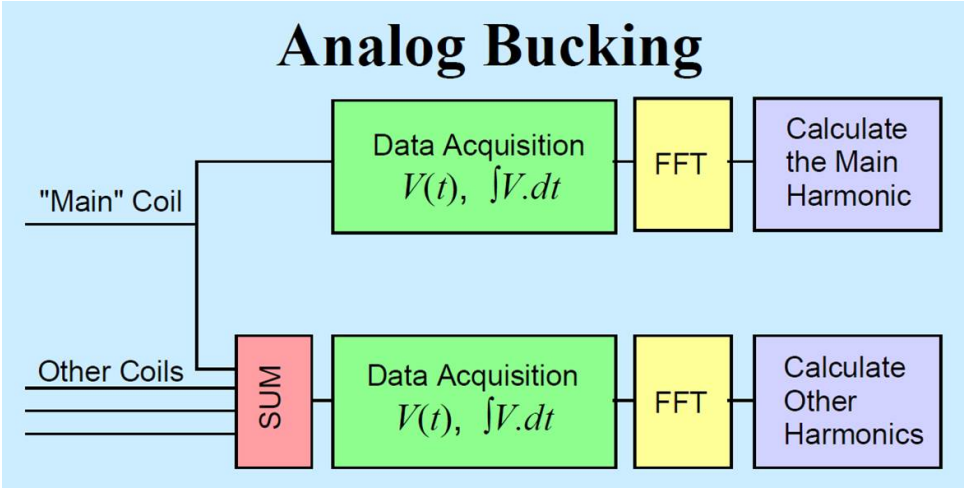

Figure 3.18: Schematic of analog bucking [9]

On the other hand, digital bucking requires coil signals to be digitized first. The results are summed up with bucking factors to null out the fundamental harmonic. The major benefit of digital bucking is the freedom in coil winding as the final sensitivity can be altered by the bucking factor. The coil combination that is impossible to achieve using analog bucking can be realized if digital bucking is applied. The error in signal due to coil construction error or other systematic errors are quantized in first FFT result and applied to the final result. The drawback is cost of required number of channel in data transmission and acquisition. Also, the ADC full scale is dictated by strength of fundamental harmonic so the erroneous harmonic may suffer to low resolution and ADC noise.

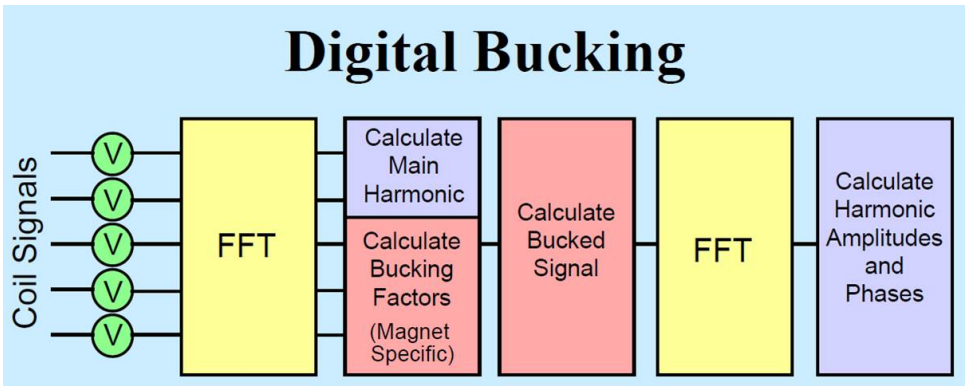

Figure 3.19: Schematic of digital bucking [9]

For the same outer radius, tangential coil has better sensitivity at higher order harmonic. This is beneficial since the precision limit is based on the small erroneous higher order harmonic. The choice of opening angle depends on the maximum harmonic of interest. For 10^{th} harmonic, the 18 degree tangential coil has the best sensitivity. The 15 degree one is good for 14^{th} harmonic and the 10 degree one should work for harmonic beyond 20^{th} order.

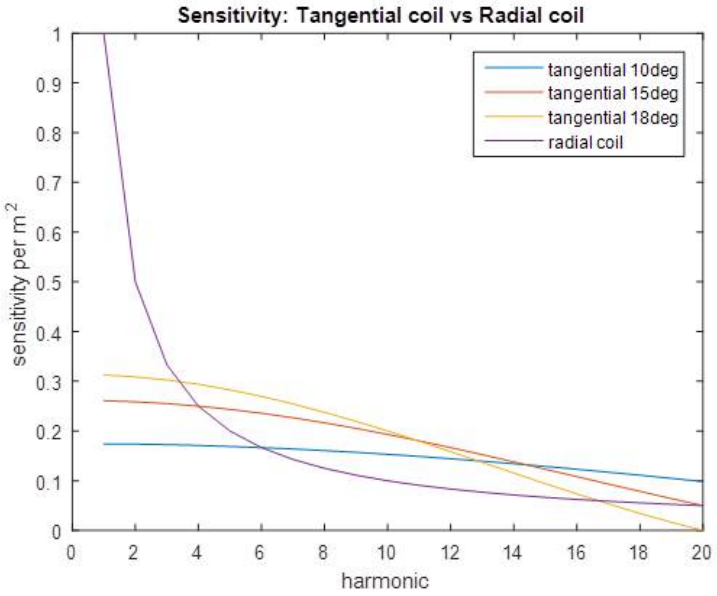

Figure 3.20: Sensitivity of $1m^2$ coil area for radial coil and tangential coil with 10, 15, and 18 degree opening.

Bucking requires at least two coils. With more coil, the desired bucking can be achieved easier. The coil parameters are calculated by solving the equation(s) $K_n = 0$ for all desired

bucking harmonic n. For example, to buck quadrupole and dipole harmonic for quadrupole measurement, the following equation has to be solved for all conductors j:

$$\sum_j N_j r_j e^{i\theta_j} (-1)^j = 0$$

$$\sum_j N_j {r_j}^2 e^{i2\theta_j} (-1)^j = 0$$

RADIAL COIL WITH N=1, N=2 BUCKING

For radial coil, all the conductors lie on x axis. The equations are simplified to:

$$\sum_j N_j r_j (-1)^j = 0$$

$$\sum_j N_j {r_j}^2 (-1)^j = 0$$

For example, from a radial coil design at DESY, the coil geometry satisfies the equation [17]:

$$N_A (r_2 + r_1) - N_B (r_3 + r_4) - N_C (r_5 + r_6) = 0$$

$$N_A \left({r_2}^2 - {r_1}^2\right) - N_B \left({r_4}^2 - {r_3}^2\right) - N_C \left({r_6}^2 - {r_5}^2\right) = 0$$

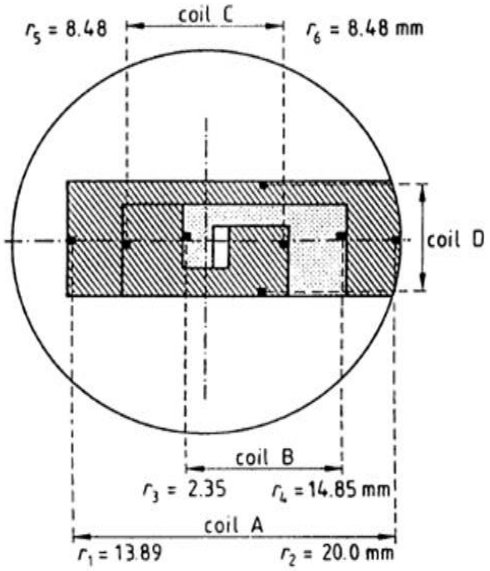

Figure 3.21: Design of radial coil for quadrupole measurement for HERA collider with dipole and quadrupole bucking [13].

TANGENTIAL COIL WITH N=1, N=2 BUCKING

For tangential coil, all the conductors lie on the same circle. As mentioned before, digital bucking is used in this coil design so each coil has an extra multiplier f. The sensitivity equations become:

$$\sum_j f_j N_j e^{i\theta_j}(-1)^j = 0$$

$$\sum_j f_j N_j e^{i2\theta_j}(-1)^j = 0$$

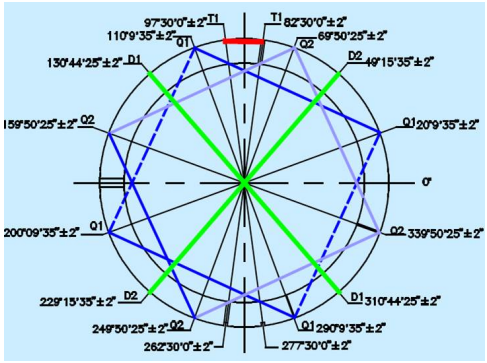

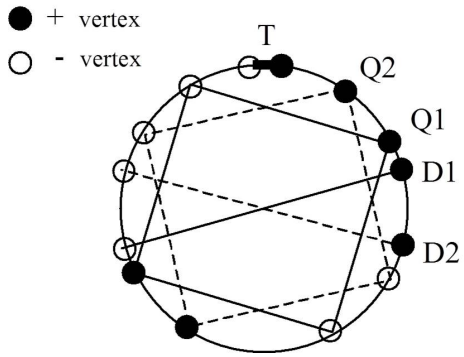

Figure 3.22: Tangential coil design at BNL with dipole and quadrupole bucking [9] (Left). Vertex diagram of each tangential coil [13] (Right).

The main coil has opening angle of 15 degree. Its sensitivity is good for harmonic from dipole to 14^{th} harmonic. The bucking coils are Morgan coil for dipole and quadrupole. Theoretically, one Morgan coil for each bucking harmonic would be sufficient. The overall sensitivity can be optimized with more bucking coils.

3.7.7 COIL FINITE SIZE ERROR

In calculation of sensitivity factors, geometry of coil is simplified as N conductor segments superimposed at the same ideal position. A better approximation of flux exposure of N segment coil is to replace the ideal position by the center of mass position of winding pattern.

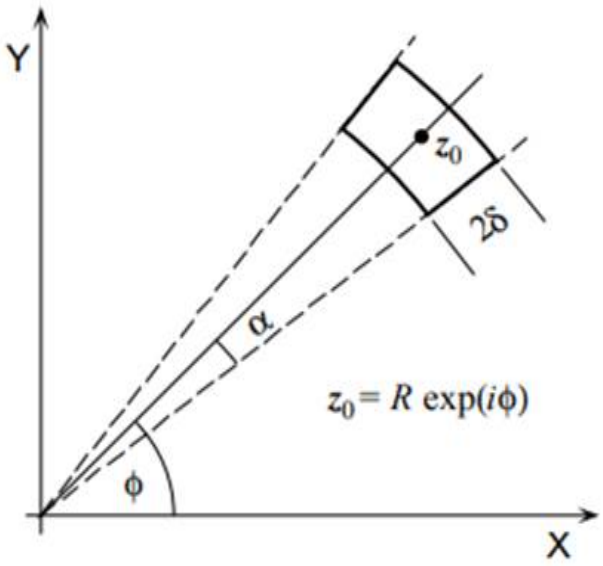

Figure 3.23: Sector shape winding at complex location z0 with boundary of winding [17].

Figure 3.23 shows a sector shape winding pattern. The center of mass position of this strand of conductor segments is [17]:

$$\left(Re^{i\phi}\right)_{C.M.}{}^{n} = \frac{\int_{R-\delta}^{R+\delta} r^n dr \int_{\phi+\alpha}^{\phi+\alpha} e^{in\phi} d\phi}{(2\alpha)(2\phi)}$$

$$= \left(Re^{i\phi}\right)^n \frac{\sin(n\alpha)}{n\alpha} \frac{\left[\left(1+\frac{\delta}{R}\right)^{n+1} - \left(1-\frac{\delta}{R}\right)^{n+1}\right]}{2(n+1)\left(\frac{\delta}{R}\right)}$$

$$= \left(Re^{i\phi}\right)^n \left[\frac{n\alpha - \frac{1}{6}(n\alpha)^3 + \dots}{n\alpha}\right] \frac{\left[2(n+1)\left(\frac{\delta}{R}\right) + \frac{2(n+1)(n)(n-1)}{3!}\left(\frac{\delta}{R}\right)^3 + \dots\right]}{2(n+1)\left(\frac{\delta}{R}\right)}$$

$$\approx \left(re^{i\phi}\right)^n \left[1 - \frac{1}{6}n^2\alpha^2\right]\left[1 + \frac{n(n-1)}{6}\left(\frac{\delta}{R}\right)^2\right]$$

Both attenuating and amplifying terms are proportional to $O(n^2)$. Therefore, when α and $\frac{\delta}{R}$ are close to each other, the error due to finite sizing can be minimized. Choosing a single loop coil can bypass these geometric errors with the trade-off of signal strength. However, the signal needs amplification by hardware or digitization at high resolution digitizer and low noise. The corrected K_n with coil finite size error is:

$$K_n = N\frac{Lr_0}{n}\left(\frac{r}{r_0}\right)^n e^{in\alpha}\left[1 - \frac{1}{6}n^2\alpha^2\right]\left[1 + \frac{n(n-1)}{6}\left(\frac{\delta}{R}\right)^2\right]$$

CHAPTER 4

CONCEPTUAL DESIGN

Argonne National Lab's rotating wire approach is adapted because of the simplicity. As mention before, single rotating wire has the simplest and expandable coil geometry. It also has less vibration during rotation due to negligible sag. As a single conductor coil, it's immune to finite size error and winding uncertainty. The low resistance also reduces the Johnson noise [13].

The drawback is the measurement time since each harmonic has to be measured individually. The rotation speed needs to be wisely chosen. Calibration work has to take place every time when wire is disassembled. The hardware requirement is also high. For this approach to work, the rotation stage pair has to be well aligned and synchronized. A Lock-in amplifier is necessary to recover the wire signal.

At Radiabeam Technologies, the Newport XPS series motion controller from 3D Hall probe system has room for two more axes. Also, a Zurich HF2LI Lock-in amplifier is already in service for the vibrating wire system. Because the Zurich Lock in amplifier provides two input channels, it makes bucking possible for only one harmonic. To buck two harmonic simultaneous, the bucking coil needs to be designed properly. Two bucking coils with proper sensitivity and number of turns will be connected in series. In this thesis, a coil is designed for the EMQD-280-709 quadrupole magnet characterization but the measurement concept

can be generalized to any type of magnet measurement.

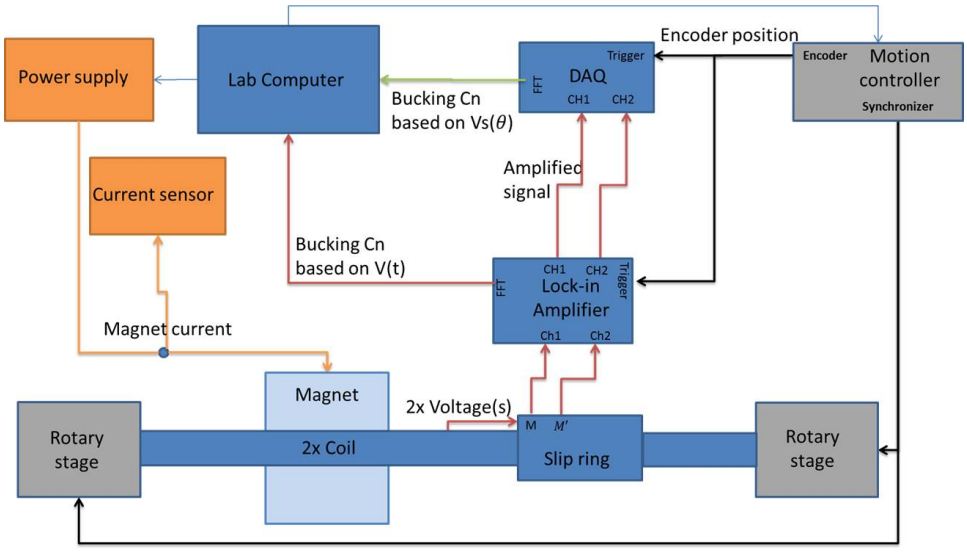

Figure 4.1: Flow diagram of rotating wire system with bucking.

Here is the introduction of components in the proposed system:

- Coil: One main coil measures harmonic content and one bucking coil provides bucking signal for calibration, alignment, and harmonic content measurement.
- Lab computer: Control current in magnet. Control motion of rotary stage via motion controller. Display and store measurement data from DAQ and Lock-in amplifier. Conduct a measurement script.
- Power supply: Generate current to excite magnetic field in electromagnet.
- Current sensor: Record current in magnet all the time.
- Motion controller: Control motion of two rotary stages for synchronized motion. Send out encoder signal to Lock-in Amplifier and DAQ.
- Rotary stage: Drives the rotor part and rotating coil (wire).
- Slip ring: Transmit electrical signal from rotor terminal to static terminal.
- Lock-in amplifier: Read encoder signal and use it as reference signal. Amplify voltage signal of individual harmonic from slip ring and perform FFT analysis. Output amplified voltage signal to DAQ.

- DAQ: Measure amplified voltage signal from Lock-in amplifier. Measure time interval between each rotary encoder count. Perform time integration and FFT analysis.

4.1 COIL

4.1.1 COIL DESIGN AND SENSITIVITY

For good sensitivity in higher order harmonics, tangential design is chosen for both main and bucking coils. The design is optimized for quadrupole measurement, which means the harmonic sensitivities other than quadrupole after bucking are maximized. Due to the channel limit in Lock-in amplifier, the quadrupole bucking coil and dipole bucking coil has to be connected in series to buck both harmonic simultaneously. An alternative quick solution would be purchasing one more amplifier channel. The main coil (M) has 15 degree opening is center at 0 degree position. The quadrupole bucking coil (QB) has 75 degree opening is center at 180 degree position. The dipole bucking coil (DB) has 180 degree opening angle at 180 degree position. M coil and QB coil are single turn and have radial size of 24mm. DB has two turns and the radial size is 13.2mm . Figure 4.2 shows the position and polarity of vertex for all coils. The length of coil is chosen as 0.5m, which is more than twice of magnetic length for EMQD-280-709. This should be sufficient to cover the entire fringe field.

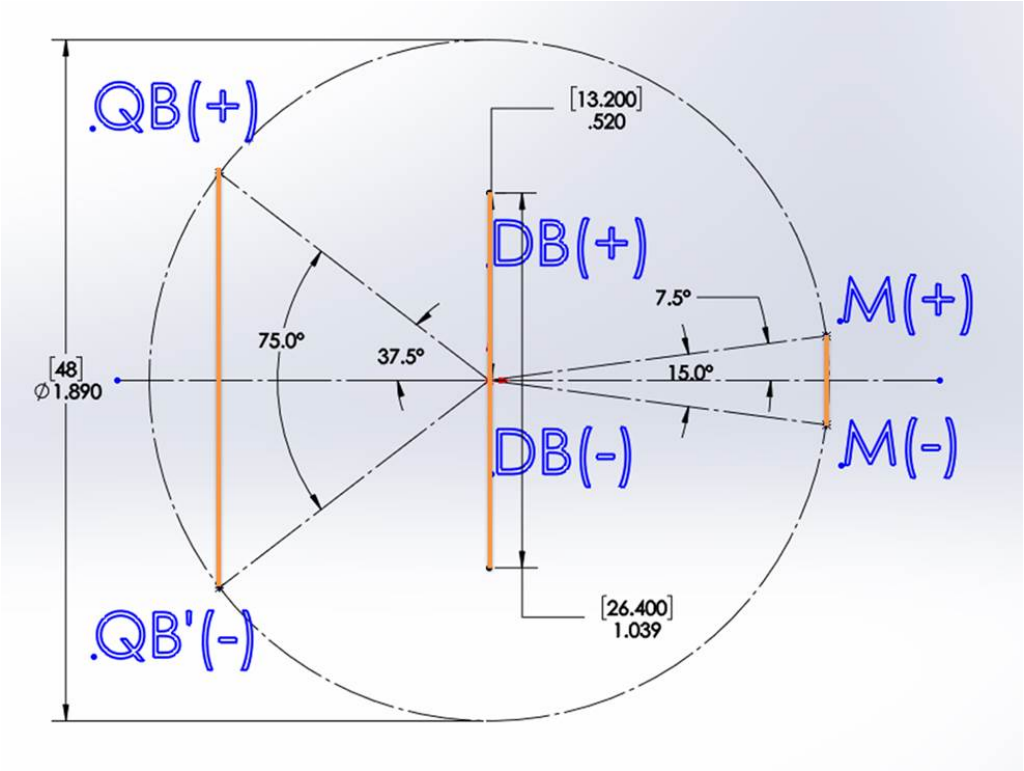

Figure 4.2: Vertex position of main coil, quadrupole bucking coil, and dipole bucking coil on a 48mm diameter circle.

Recalled that sensitivity for single turn tangential coil is expressed as:

$$K_n = \frac{2Lr_0}{n}\left(\frac{r}{r_0}\right)^n \sin\left(\frac{n\delta}{2}\right) e^{in\alpha}$$

The sensitivity for main coil and bucking coils are:

$$Main\ K_n = \frac{2(0.5m)(0.024m)}{n}\sin\left(\frac{n\pi}{24}\right)$$

$$QB\ K_n = \frac{2(0.5m)\,(0.024m)}{n}\sin\left(\frac{n\pi}{4}\right)\ (-1)^n$$

$$DB\ K_n = 2 * \frac{2(0.5m)\,(0.0132m)}{n}\sin\left(\frac{n\pi}{2}\right)\ (-1)^n$$

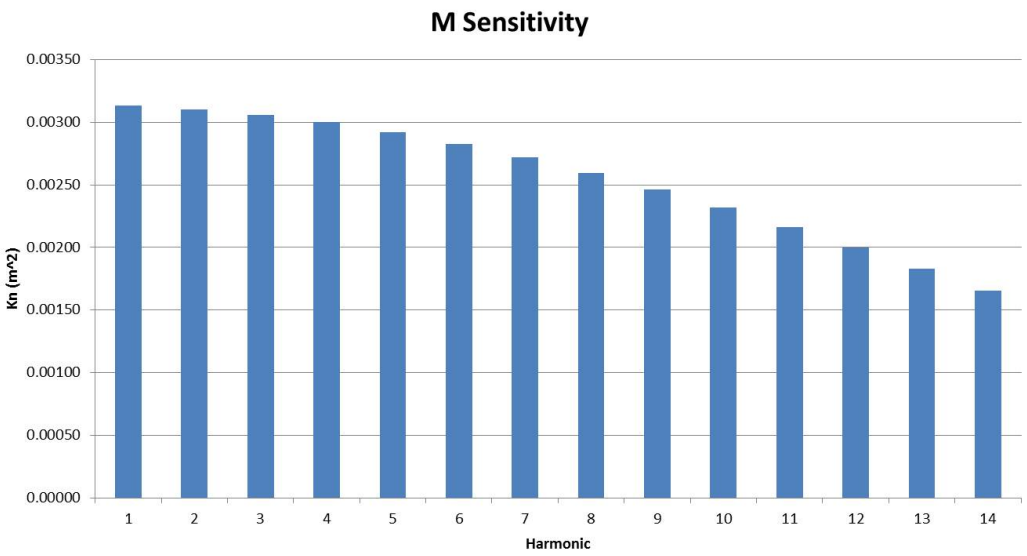

Figure 4.3: Sensitivity of main coil.

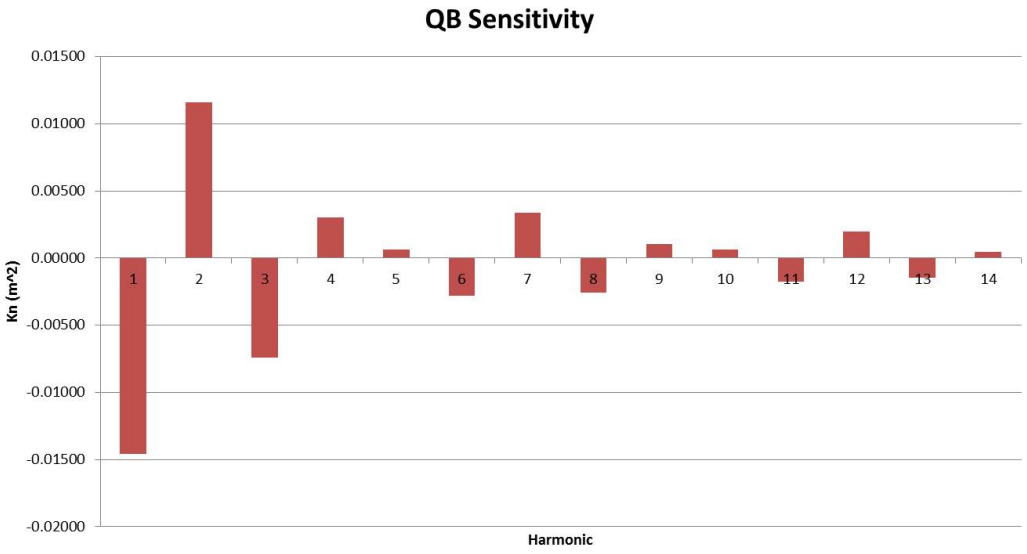

Figure 4.4: Sensitivity of quadrupole bucking coil for quadrupole magnet measurement.

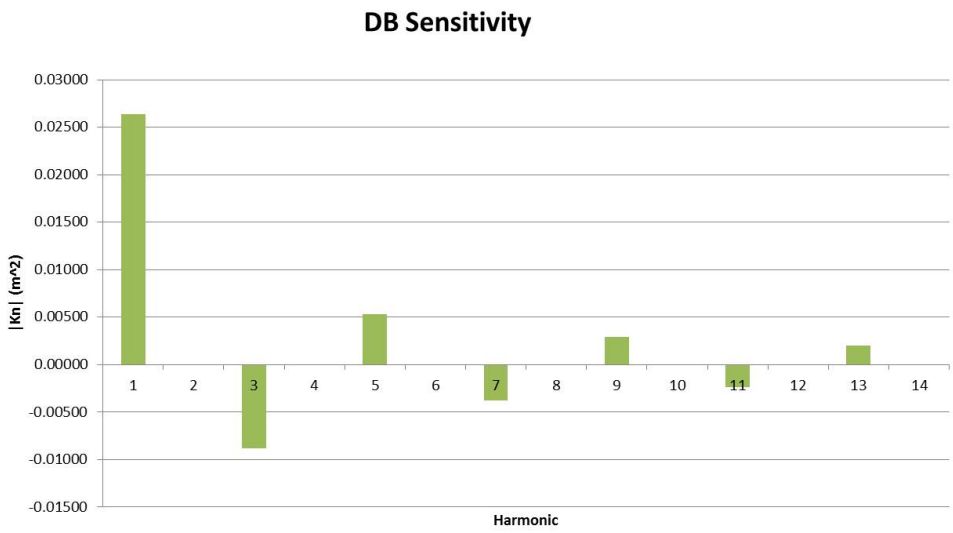

Figure 4.5: Sensitivity of dipole bucking coil for quadrupole magnet measurement.

The derivation for the DB coil is tricky. Since there's only one channel for bucking, QB coil and DB coil will share the same bucking factor. QB coil is chosen as the master bucking coil. So the bucking factor is derived from main coil and QB coil. For nth harmonic digital bucking, the bucking factor needs to satisfy the equation:

$$Main\ K_n + f_n * QBK_n = 0$$

The bucking factor is calculated as:

$$f_n = -\frac{Main\ K_n}{QBK_n} = \frac{\sin\left(\frac{n\pi}{24}\right)}{\sin\left(\frac{n\pi}{4}\right)}(-1)^{n+1}$$

DB coil is designed to suppress the residual dipole sensitivity when QB coil is bucking quadrupole sensitivity. DB coil's design parameter is calculated by solving:

$$Main\ K_2 + f_2 * QBK_2 + f_2 * DBK_1 = 0$$

DB coil as the Morgan coil for dipole, has no contribution on quadrupole sensitivity. Solving the equation, the radial size and number of turns for DB coil is found as 13.2mm and 2 turns, respectively.

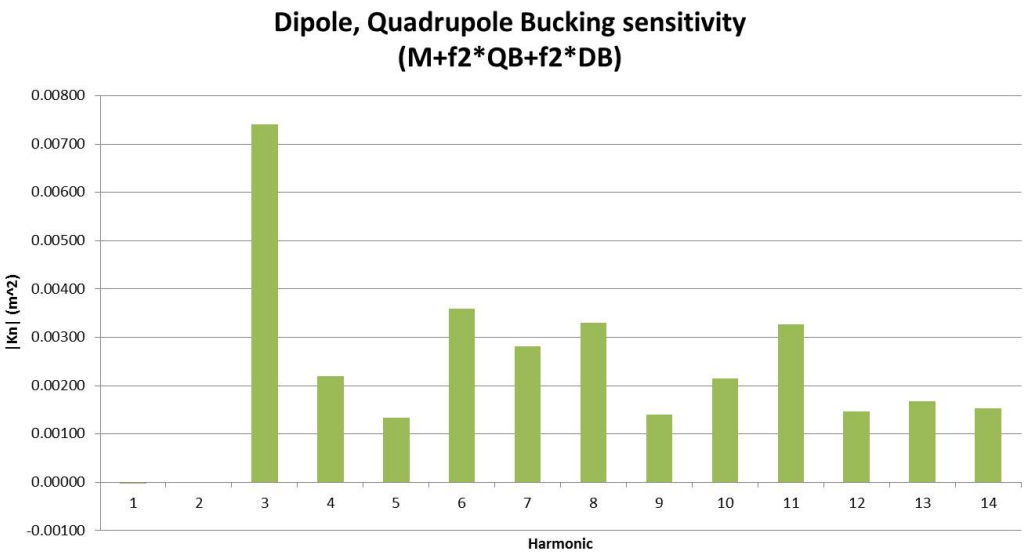

Figure 4.6: Overall sensitivity of coil when dipole and quadrupole bucking is active.

Although the combination of QB and DB works out for duel harmonic bucking, the coupling between QB and DB coil make it impossible to correct the manufacture error between them. The detail for sensitivity and bucking factor is shown in Table 4.1. The minimum sensitivity is 0.00134m^2 for 5^{th} harmonic.

Table 4.1: Starting from left to right, each column shows the value of: harmonic order, main coil sensitivity, QB coil sensitivity, bucking factor, DB coil sensitivity, and QB+DB coil sensitivity, active dipole quad bucking sensitivity.

n	M	QB	fn	DB	QB+DB (in series)	Dipole+Quad bucking
						$M+f_2*QB+f_2*DB$
	$[m^2]$	$[m^2]$		$[m^2]$	$[m^2]$	$[m^2]$
1	0.00313	-0.01461	0.21441	0.02640	0.01179	-0.00003
2	0.00311	0.01159	-0.26795	0.00000	0.01159	0.00000
3	0.00306	-0.00739	0.41421	-0.00880	-0.01619	0.00740
4	0.00300	0.00300	-1.00000	0.00000	0.00300	0.00220
5	0.00292	0.00063	-4.66390	0.00528	0.00591	0.00134
6	0.00283	-0.00283	1.00000	0.00000	-0.00283	0.00359
7	0.00272	0.00340	-0.80020	-0.00377	-0.00037	0.00282
8	0.00260	-0.00260	1.00000	0.00000	-0.00260	0.00329
9	0.00246	0.00102	-2.41421	0.00293	0.00395	0.00140
10	0.00232	0.00062	-3.73205	0.00000	0.00062	0.00215
11	0.00216	-0.00173	1.24969	-0.00240	-0.00413	0.00327
12	0.00200	0.00200	-1.00000	0.00000	0.00200	0.00146
13	0.00183	-0.00146	1.24969	0.00203	0.00057	0.00168
14	0.00166	0.00044	-3.73205	0.00000	0.00044	0.00154

4.1.2 CALIBRATION

Calibration requires measurement on a known magnetic source with known harmonic content and skew angle. The best option is dipole because it's the simplest form of field. It can be easily cross-checked by other type of measurement (for example, NMR probe) to increase accuracy and confidence. First, the dipole needs to be setup properly. In the proposed system, 90 degree of rotatory stage is point up (opposite direction of gravity). So the field direction of dipole should be aligned to gravity as well. The motion of rotating coil should

be inside of dipole's good field region all the time. The calibration process measures dipole field in dipole bucking mode. The result for dipole if often not zero due to error in wire position. It could indicate a construction error in coil or the non-concentricity between coil and rotation axis. A new bucking factor F_2 can be calculated. Applying the $-F_2$ to bucking factor can doubles dipole harmonic and gives better calibration accuracy. The calibration factor is measured as:

$$Scale\ factor = \frac{|C_1|_{reference}}{|C_1|_{measured}}$$

$$Zero\ angle = \varphi_{\ measured} - \frac{\pi}{2}$$

The correction needs to be applied on the final harmonic content result.

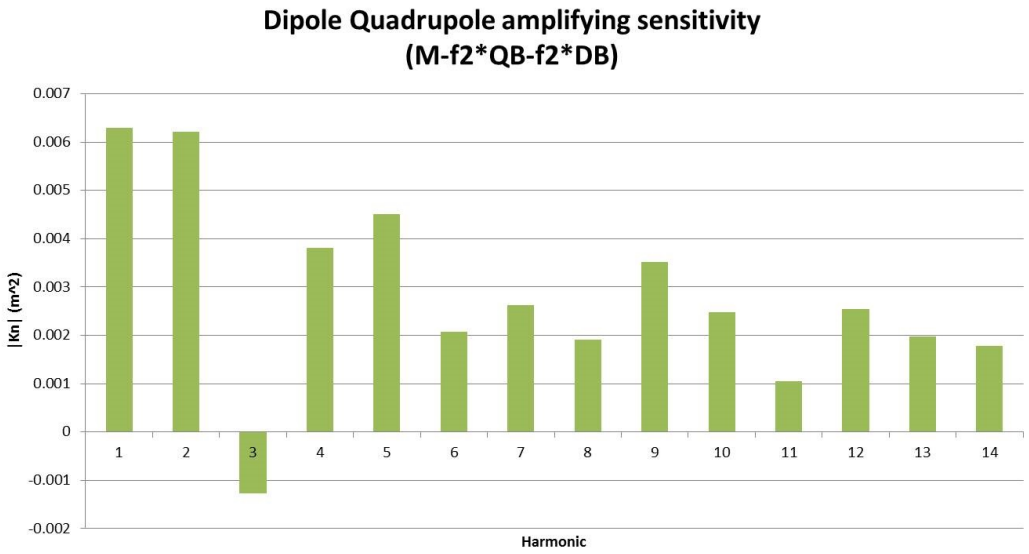

Figure 4.7: Sensitivity of coil when -f_2 is used as bucking factor. Dipole and quadrupole are amplified to twice.

4.1.3 ALIGNMENT

Spill down field error is used to align the magnet. If the axis of rotation is off by distance Δr, we have

$$\frac{\Delta C_{n-1}}{(n-2)!}\left(\frac{\Delta r}{r_0}\right)^{n-2} = \frac{\Delta C_n}{(n-1)!}\left(\frac{\Delta r}{r_0}\right)^{n-1}$$

$$\Delta C_{n-1} = \frac{\Delta C_n}{n-1}\left(\frac{\Delta r}{r_0}\right) \tag{4.1}$$

As the spill-down harmonic of quadrupole, the dipole field is expressed as:

$$\Delta C_1 = \Delta C_2\left(\frac{\Delta r}{r_0}\right)$$

or

$$\Delta B_1 = \Delta C_2\left(\frac{\Delta x}{r_0}\right)$$

$$\Delta A_1 = \Delta C_2\left(\frac{\Delta y}{r_0}\right)$$

When magnet is aligned to rotation axis, ΔB_1 and ΔA_1 becomes zero. To conduct this alignment procedure, the same bucking factor –F_2 is used. The dipole harmonic of testing quadrupole magnet can be measured with twice of sensitivity, which increases the accuracy.

4.1.4 MATERIAL AND POSITIONAL TOLERANCE

The chosen wire is 32 AWG, heavy build wire made by MWS Wire Industry [18]. The OD of wire is ∼0.01". Resistance for each coil is less than 1Ohm for 0.5m length. The Johnson noise for each coils are about 0.01uV at 10 kHz sampling rate. The coil fixture is a simple rectangular plate made of any easy machines material. If metal is used, insulation will be required under terminal. The tension-applying feature isn't added yet. The edge that wire stays on is rounded to prevent wire breaking.

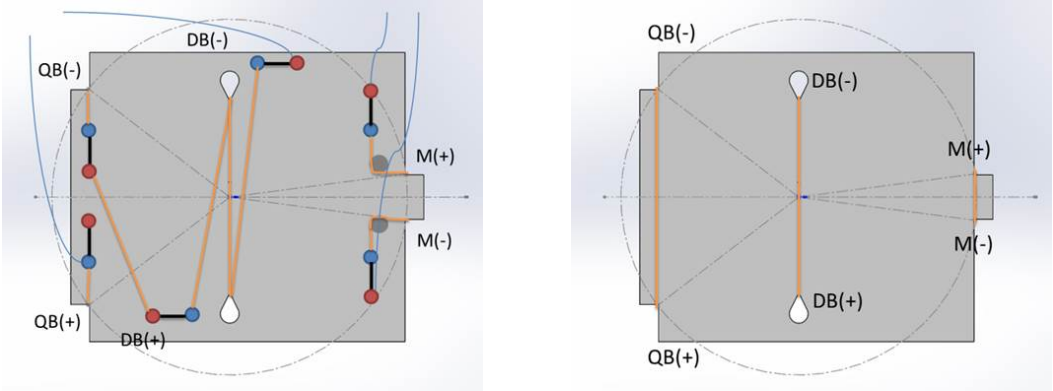

Figure 4.8: Coil fixture near slip ring. The wire ends on terminal with tension. The connection between terminal and slip ring is done by other wire (Left). Coil fixture away from slip ring (right).

The wire position is controlled by the position of cut at four corners. A reasonable tolerance of wire position for radial dimension is 0.001", which give a relative error of ∼0.1%. For angle, 0.5 degree (∼10mrad) angular error tolerance is selected. The systematic error in sensitivity corresponds to these dimensional errors estimated by:

$$\left|\frac{\Delta K_n}{K_n}\right|_{syst} = \sqrt{\left(n\frac{\Delta r}{r}\right)^2 + (in\Delta\alpha)^2 + \left(\frac{n}{2}\cos\left(\frac{n\delta}{2}\right)\Delta\delta\right)^2}$$

$$\leq n * \sqrt{\left(\frac{\Delta r}{r}\right)^2 + (i\Delta\alpha)^2 + \left(\frac{1}{2}\Delta\delta\right)^2} \approx n * 0.01 \; per \; coil$$

Angular error has the most contribution. The bucking coil has three loops, so the error is n*0.03 instead. For both main and bucking coil, the total systematic error in sensitivity is

$$n * \sqrt{(0.01)^2 + (0.03)^2} \approx n * 0.03$$

Although the systematic will be calibrated, it's calibrated in dipole. The residual error in calibration easily scaled up with harmonic order. Therefore calibration needs to be done with highest possible resolution. The scale factor acquired from calibration must be evaluated to 6 significant digits for unit (10^{-4}) level accuracy.

On the other hand, the random error in wire position should be considered as motion error in wire. The rotary stage has 1.5um eccentricity and 0.005 degree accuracy. The random error in sensitivity is estimated by:

$$\left|\frac{\sigma_{K_n}}{K_n}\right|_{random} = \sqrt{\left(\frac{n(n-1)}{2}\left(\frac{\sigma_r}{\overline{r}}\right)^2\right)^2 + \left(\frac{n^2}{2}{\sigma_\alpha}^2\right)^2} \approx n^2 * 4.3ppb \; per \; conductor \; segment$$

The main coil has two conductor segments, so the random error is $\frac{1}{2}n^2 * 4.3ppb \approx n^2 * 2ppb$. The bucking coil has six conductor segment, so the random error $\frac{1}{6}n^2 * 4.3ppb \approx n^2 * 0.7ppb$. The total random error in sensitivity is:

$$n^2 * \sqrt{(2)^2 + (0.7)^2}ppb \approx n^2 * 2.1ppb$$

4.2 MECHANICAL MODEL AND DRAWING

The conceptual designed is modeled in SolidWorks 3D. The mechanical design will be finished by engineer at Radiabeam Technologies.

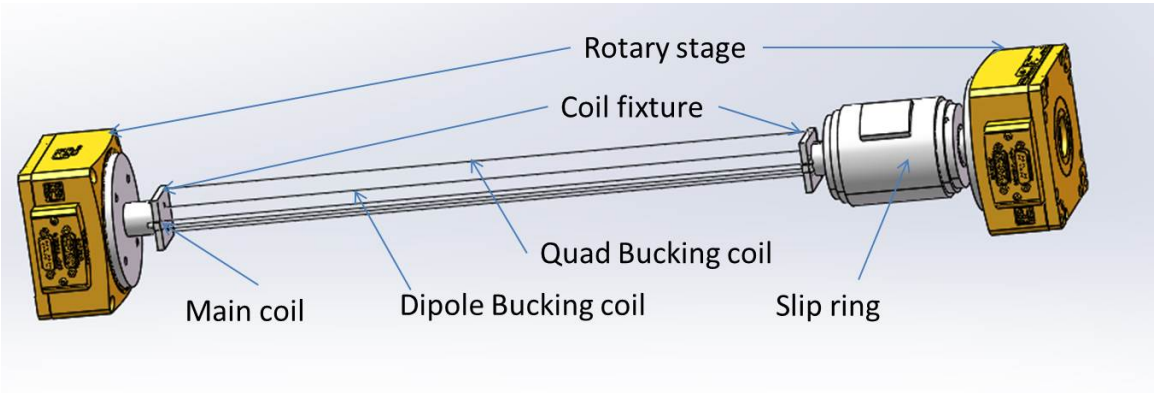

Figure 4.9: Side view of conceptual design of assembly.

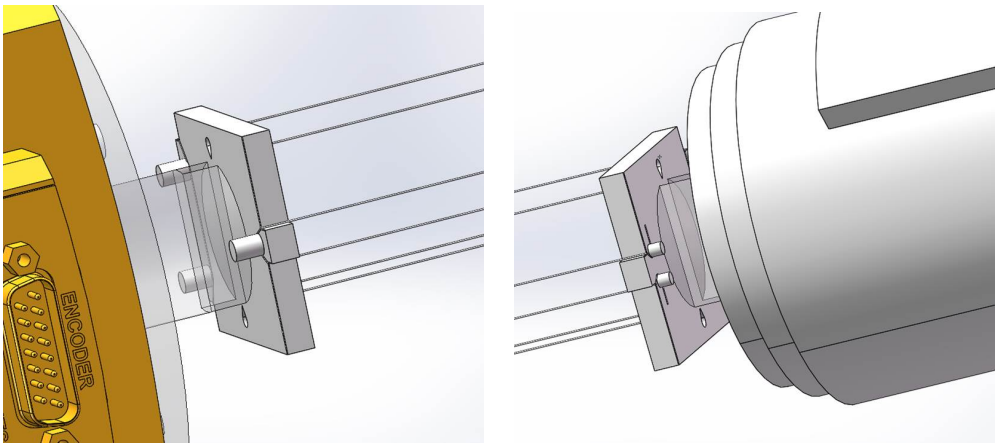

Figure 4.10: Zoom in of coil fixture and wire at far away side (Left) and slip ring side (Right).

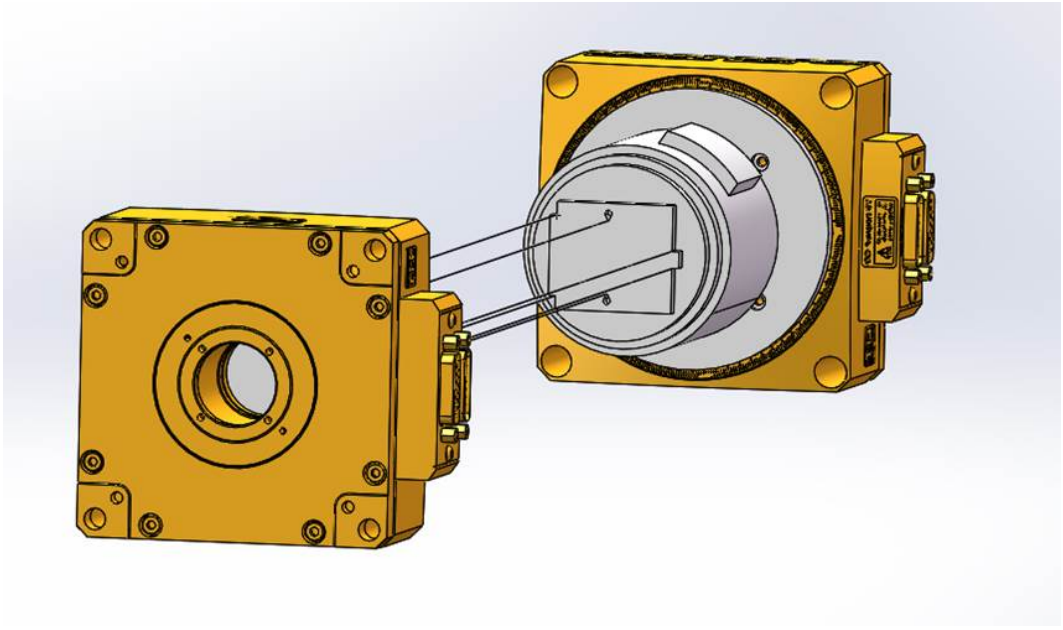

Figure 4.11: Angle view of conceptual design assembly.

4.3 HARDWARE SECTION LIST

Table 4.2: Hardware purchase list

Hardware	Brand	Model	Unit needed	Unit price	Leadtime
Lock-in Amplifier	Zurich	HF2LI	1	N/A	N/A
DAQ	National Instrument	PXIe-4309	1	$6,663	2 week
Rotary stage	Newport	RGV-100 BL	2	$6,546	In-stock
Slip ring	Merdian Laboratory	MXT4/HD	1	$3,990	5-6 week

4.3.1 ROTARY STAGE: NEWPORT RGV-100 BL WITH ENCODER

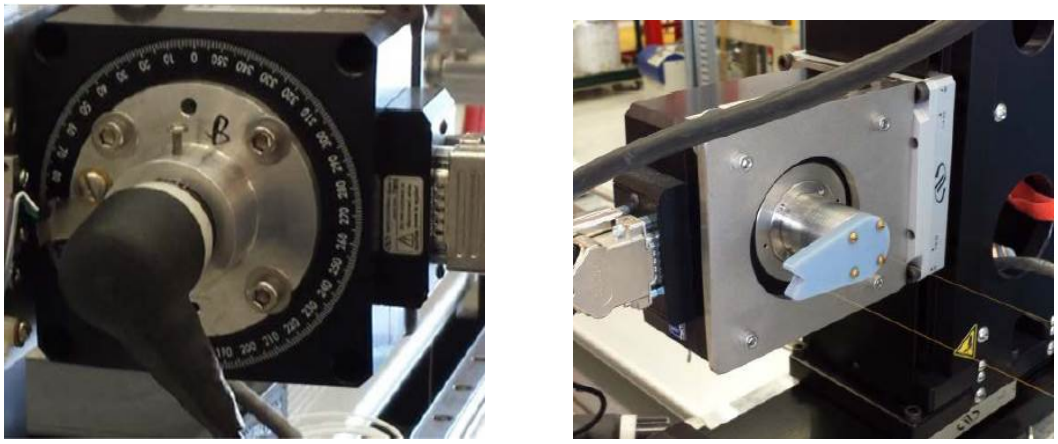

Figure 4.12: Newport RGV-100BL at ANL [7]. Front view(Left) and Back view (Right)

The first critical requirement for rotating wire is the synchronized rotation at both ends. Poorly synchronized rotation results in deformation in coil geometry. The error builds up in time and could finally fail the experiment. The range and stability rotation speed is less critical because they can be fixed by signal amplification and time integration. Newport RGV-100 BL [19] rotary stages used in ANL rotating wire is chosen. The synchronization is realized by Newport XPS motion controller [20] which Radiabeam already own. The stage

has 2 rps maximum rotating speed. Eccentricity is ±1.5um. Rotation speed stability is not specified but should be decent enough. Maximum encoder resolution is 15000 counts per revolution. The zero-angle is used as the reference angle for harmonic measurement. The repeatability of returning to this origin is 0.0001 degree. From the eccentricity 1.5um, the transverse vibration error can be estimated by:

$$\frac{\Delta C_m}{C_2} = \left(\frac{K_1}{K_m}\right)\frac{1.5um}{24mm} = \left(\frac{K_1}{K_m}\right)63ppm = \frac{0.00003}{0.00134}63ppm = 1.4ppm$$

In worst case scenario, if $K_1$is larger by 0.03 and K_5 is smaller by 0.16 due to manufacture error and calibration didn't happened, the worst transverse vibration error is 1.7ppm.

In the proposed system, the default rotation speed is picked at 1rps. Only 1000 counts per revolution will be used in triggering to reduce DAQ time resolution. The sampling rate for coil signal is set at 10kHz for guarantee triggering. Speed stability needs to be tested during commission. Assuming the torsion vibration is 0.1 degree. The equivalent error in harmonic content can be estimated by:

$$\frac{\Delta C_m}{C_2} = 2 * \left(\frac{K_2}{K_m}\right)270ppm$$

However, the bucking factor is calculated by K_2. Therefore the bucking is nearly perfect, regardless of manufacture error. The torsional vibration error is negligible.

4.3.2 ZURICH HF2LI LOCK-IN AMPLIFIER

Figure 4.13: Zurich HF2LI Lock-in amplifier at Radiabeam Technologies.

Lock-in amplifier plays the most important role in rotating wire approach. The signal collected by single wire is very small (10nV level). When the signal is smaller than conventional amplifier's internal noise level, the signal is not resolvable regardless of any gain setting. Lock-in amplifier use phase-sensitive detector that detects signal with typically x10^6 narrower bandwidth [21]. The signal is can be recovered to x1000 larger. HF2LI lock-in amplifier [22] has 120dB dynamic reserve can recover signal that is x10^{-6} smaller than its input noise. At 10 kHz sampling rate, the minimum resolvable signal strength would be

$$2 * \frac{5nV}{\sqrt{Hz}} * \sqrt{10000Hz} * 10^{-6} = 1pV$$

The input resolution is 14 bit and the minimum scale is 1nV so the resolution is fine enough to support the 1pV precision. Despite the powerful precision, the resolved signal is vulnerable to background noise such as electrical noise from stepper motor and slip ring resistance. These noises will cause systematic error in the FFT result. In measurement, HF2LI receive encoder signal from motion controller as reference to measure each harmonic,

one at a time. For example, dipole harmonic will be measured with the one rotation frequency. Assuming the harmonic content up to 14^{th} order is measured with 1 rps rotation speed, the total scan time would be 14 seconds. The measurement is still very efficient. HF2LI perform FFT on voltage signal. The accuracy is dependent to the consistency of rotational speed. If flux-based analysis is necessary, HF2LI can output a 10V signal with 16 bit resolution.

4.3.3 DAQ: NI PXIE-4309

Figure 4.14: National instrument NI PXIe-4309 flexible resolution PXI analog input module.

NI PXIe-4309 [23] is used if the rotation speed is too inconsistent to use voltage signal. NI PXIe-4309 has 28bit resolution, 23ppm gain error, and 50ppm timing accuracy at 10 kHz sampling rate and 10V range. The trigger pulse width is 20ns with 50ppm accuracy. At 1 rps rotation speed and 1000 count/rev encoder setup, the time interval between trigger is 1ms. Using the error propagation formula, the accuracy of voltage-time signal should be

$$\sqrt{(23ppm)^2 + (\frac{20ns}{1ms})^2} \approx 30ppm$$

At the same acquisition setup, the 3-sigma input noise is 18uV, which gives the resolution

in signal strength to be 2*18uV=60uV. When the input signal of fundamental harmonic is amplified to 10V, the theoretical minimum resolvable harmonic content for other harmonics is:

$$\frac{36uV}{10V} = 3.6\ ppm$$

However, the final resolution is limited by the 16 bit output resolution from Lock-in amplifier, which is equivalent to ∼15 ppm or 0.15 units. This precision is decent enough.

4.3.4 SLIP RING: MERDIAN LABORATORY MXT4/HD

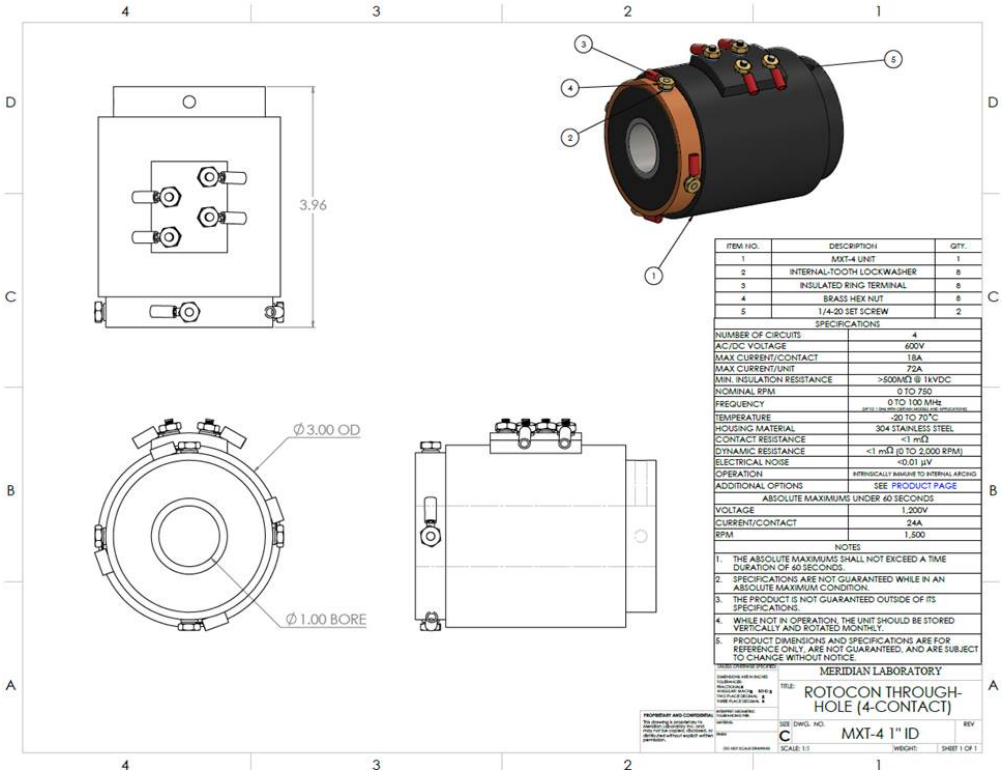

Figure 4.15: Engineering drawing for Merdian Laboratory MXT4/HD slip ring. Electrical noise <0.01uV. Maximum speed=750rpm. Resistance <0.01Ohm.

The slip ring transmit signal from rotation frame to static frame by direct contact, mercury contact, or induction. The noise contribution in this device needs to be emphasized because the noise is likely coupled with rotation. The fake signal from this noise cannot be removed by averaging and is hard to be distinguished from correct signal. Among the three

options, the mercury contact way is chosen because of the low noise and low resistance benefits. Merdian Laboratory MXT4/HD has 0.01uV electrical noise and <0.1mOhm contact resistance. The max speed 750rpm serves our application.

4.4 PROPOSED SYSTEM SPECIFICATION

Parameter of EMQD-280-709 magnet is used to design the coil. The radial size of main coil and quadrupole bucking coil are the same as the reference radius 24mm. The coil length is 500mm so all fringe field is covered. The default parameters for operation are the 1 rps rotation speed, 10 kHz sampling rate and, 1000 triggers per revolution. The highest harmonic to measure is the 14^{th} harmonic. The accuracy and precision are estimated by systematic error and random error or noise [24]. Repeatability can only be examined based on real measurement.

4.4.1 ACCURACY

From error propagation section, we know the system accuracy is controlled by the data acquisition accuracy and systematic error in coil manufacture. The harmonic content and its relative error due to error from six sources are expressed as:

$$|C_n| = \left| \frac{FFT\left(Vs\right)_n}{NK_n} \right|$$

$$\left| \frac{\Delta C_n}{C_n} \right| = \sqrt{\left(\frac{\Delta_{Voltage}}{C_n} \right)^2 + \left(\frac{\Delta_{time}}{C_n} \right)^2 + \left(\frac{\Delta_{\theta}}{C_n} \right)^2 + \left(\frac{\Delta_{K_n}}{C_n} \right)^2}$$

where

$$\frac{\Delta_{Voltage}}{C_n} = gain\ error + \frac{FFT(\Delta V_{system\ noise})_n * Rotation\ period}{FFT\left(Vs\right)_n}$$

$$\frac{\Delta_{time}}{C_n} = \frac{\Delta t_{trigger}}{T/N_s}$$

$$\frac{\Delta_{\theta}}{C_n} = e^{in\Delta\theta}$$

$$\left|\frac{\Delta_{K_n}}{C_n}\right|_{syst} = \sqrt{\left(n\frac{\Delta r}{r}\right)^2 + (in\Delta\alpha)^2 + \left(\frac{n}{2}\cos\left(\frac{n\delta}{2}\right)\Delta\delta\right)^2}$$

In addition, the vibrational error also contributes to systematic error. Although they cannot be removed calibration, an active bucking measurement can minimize these errors. The transverse and torsional vibration errors are expressed as:

$$\frac{\Delta C_m}{C_n}_{transverse} = (n-1)\left(\frac{K_{n-1}}{K_m}\right)\left(\frac{D_{m-n+1}}{r_0}\right)$$

$$\frac{\Delta C_m}{C_n}_{torsional} = n\left(\frac{K_n}{K_m}\right)T_{m-n}$$

The first two terms are calculated in Section 4.3.3. The accuracy of signal acquisition is:

$$\sqrt{(23ppm)^2 + (\frac{20ns}{1ms})^2} \approx 30ppm$$

Notice that the system noise error in voltage signal error is not included for now because it can only be acquired by background measurement during commission. The third term can be removed by performing measurement in both rotation directions. The forth term is calculated in Section 4.1.4. The accuracy limit due to manufacture error in coil is:

$$n * 0.03$$

where n is the order of harmonic. The fifth and sixth terms are discussed in section 4.3.1. The effect of transverse vibration due rotary stage's eccentricity is estimated as 1.4ppm in worst case scenario (n=5). The effect of torsional vibration is zero due to digital bucking treatment.

The known overall system accuracy is:

$$\sqrt{(30ppm)^2 + (n * 0.03)^2 + (1.4ppm)^2} \approx n * 0.03$$

It's clear that the coil manufacture error controls the overall error in harmonic content accuracy. When calibration is properly done, the accuracy of system should be reduced to

~30ppm plus the accuracy of calibration source. At Radiabeam, the most accurate magnetic field sensor is SENIS F3A Hall probe [25], which has 0.1% accuracy. The calibrated accuracy of system would be:

$$\sqrt{(30ppm)^2 + 0.1\%^2} \approx 0.1\%$$

The accuracy can be improved with better reference measurement device. Typical NMR probe with ppm level accuracy can greatly improve the accuracy to 30ppm. There are unknown sources of systematic error that need to be evaluated during commission.

4.4.2 PRECISION

We know the harmonic content is calculated by the voltage or flux signal being measured and the coil sensitivity. The precision of $|C_n|$ cannot be better than precision of $FFT\,(Vs)_n$ and precision of K_n.

$$|C_n| = \left|\frac{FFT\,(Vs)_n}{NK_n}\right|$$

$$\left|\frac{\sigma_{C_n}}{C_n}\right| = \sqrt{\left(\frac{\sigma_{Voltage}}{C_n}\right)^2 + \left(\frac{\sigma_{time}}{C_n}\right)^2 + \left(\frac{\sigma_{Kn}}{C_n}\right)^2}$$

At 10 kHz, the minimum resolvable signal by Lock-in amplifier is 1pV. This precision is high that it will not be the limiting factor of this system. From section 4.3.3, we know the minimum resolvable harmonic content in voltage signal is 15ppm. Assuming the random error in integration time the same as its accuracy, the second term is:

$$\frac{20ns}{1ms} = 20ppm$$

The last term is calculated in section 4.1.4. The random error in K_n is calculated as: $n^2 * 2.1ppb$. For 14^{th} harmonic (worst case), the random error is 0.4ppm. The known overall precision of this system is:

$$\sqrt{(15ppm)^2 + (20ppm)^2 + (0.4ppm)^2} \approx 25ppm$$

It means that when the fundamental harmonic is measured and presented as 10000 units, the other harmonics are precise to 0.25units. The first and second term cannot be reduced by number of measurement because they are the minimum resolution of this system. Therefore the minimum resolution of this system is 25ppm.

4.5 MEASUREMENT PROCEDURE

The example measurement procedure for quadrupole is:

1. Preparation

1.1. Setup target magnet on a kinematic stand at middle of test bench

1.2. Initialize rotary stage, verified synchronization, return to origin

1.3. Install coil fixture on rotation stage

1.4. Rough align and center the magnet with respect to rotations axis using laser

1.5. Put wire on coil fixture to create main coil, dipole bucking coil, and quadrupole bucking coil

1.6. Apply tension on each coil

2. Calibration

2.1. Setup calibration dipole around coil

2.2. Level dipole to gravity

2.3. Turn on calibration field

2.4. Connect coil terminal and slip ring terminal.

2.5. Start rotation

2.6. Measures dipole strength by M coil and QB coil

2.7. Calculate bucking factor F2

2.8. Apply -F2 bucking factor and measure dipole strength C1

2.9. Calculate scaling factor and zero-angle

2.10. Turn off calibration field and put away dipole magnet

3. Alignment

3.1. Turn on target magnet to nominal value

3.2. Apply -F2 bucking factor and measure dipole strength C1

3.3. Adjust magnet position to minimized dipole reading

3.4. Record the residual dipole field

4. Fundamental harmonic measurement

4.1. Apply -F2 bucking factor and measure quadrupole strength C2

5. Harmonic content measurement

5.1. Apply F2 bucking factor and measure nth harmonic strength Cn

5.2. Measure nth harmonic strength Cn with main coil (for comparison)

6. Repeat step 4 and 5 for different condition (Transfer function, remnant field measurement, center shift measurement)

7. Reverse rotation direction to remove minimum angle step error

8. Save measurement data

9. Correct raw data with scaling factor and zero-angle

9. Turn off motion

10. Turn off target magnet

11. Disconnect coil

12. Remove target magnet The motion control, power supply control and measurement control are done in LabView interface. The measurement in step 4 and 5 are actually done at the same time.

CHAPTER 5

SUMMARY

Quality assurance in accelerator magnet is important to ensure functionality of accelerator system and quality of experiment data. The quality of magnet is determined by the harmonic content. The harmonic content can be measured by induction, Lorentz force, and Hall effect. Among all the approaches, the rotating coil method based on induction is the most practical and efficient one. A real measurement on EMQD-280-709, a diamond shape quadrupole magnet, is performed based on 3D hall probe method. This single scan measurement takes roughly 4 hours to collect raw data that's resolvable up to only 6th order harmonic. The alignment is not included. Using rotating coil method, the measurement would finish within 30 minute with higher resolvable harmonics and more than ten times of redundant scans.

The theory of rotating coil method is thoroughly discussed in Chapter 3. The derivation starts with multipole expansion of magnetic field in cylindrical coordinate. Using the property of the periodicity in each harmonic, a harmonic decomposition method is introduced to calculate harmonic content from given field map. The field quality is then determined.

The second part of chapter 3 introduces four different types of rotating coil design and the sensitivity of each design. Due to induction, the flux variance sensed by coil is measured as voltage signal. The sinusoidal signal is then by analyzed by Fourier transformation to

come up with harmonic content. Time integration process is added to correct the effect of inconsistent rotation speed.

In the last section of chapter 3, error propagation is derived for error in signal strength, timer, angular position, and coil geometry. The effect of transverse and torsional vibration is also discussed. Because systematic error cause by vibration cannot be removed by calibration, the treatment by bucking is introduced. The bucking method requires additional coils to generate counter signal to cancel the error due to vibration. The bucking coils can be directly connected to main coil (analog bucking) or digitized by individual digitizer (digital bucking). The digital bucking approach allows re-scaling for signal strength. Therefore, coils can be designed with more freedom.

Based on technology survey in chapter 2 and current apparatus, the rotating wire approach in Argonne National Laboratory is adopted. The best feature of this approach is the simplicity in coil winding and flexibility in coil length and radial size. The challenges in this approach are the extremely low signal strength and shaft-free rotation mechanism. The first difficulty can be solved by lock-in amplifier, which typical resolves input signal at nV level by noise reduction. The second difficulty can be solved by twin rotary stage in synchronization. On top of the existed design, bucking coil is added to enable bucking capability for two harmonics simultaneously.

In chapter 4, the conceptual system of rotating wire is built. A set of coils is designed for the example quadrupole magnet. Since our lock-in amplifier model (HF2LI by Zurich Instruments) has only two input channels, the bucking coil needs to provide bucking for dipole and quadrupole harmonic simultaneously. A winding design is worked out and provides full bucking in quadrupole and 30ppm bucking for dipole harmonic. In operation, the two rotary stages (RGV 100BL by Newport Corporation) rotates at 1 rps speed. The motion controller is set to outputs encoder signal of 1000 counts per revolution to trigger

measurement in lock-in amplifier and DAQ (NI-PXIe-4309). The induced voltage signal from coil is amplified by HF2LI and output to DAQ (NI-PXIe-4309) for time integration. Both lock-in amplifier and DAQ are sampling at 10 kHz. After fast Fourier transformation, the harmonic content up to 14th order is recorded and presented in real time. The hardware specification, coil manufacture error, and operating parameter are used in error propagation. After calibration, the accuracy and precision of this proposed system are 0.1% and 25ppm, respectively. The accuracy is limited by the available reference measurement at Radiabeam in calibration process. If a NMR probe (typical accuracy is at ppm level) is used instead, the accuracy of proposed system can be improved to 30ppm at most. Lastly, a procedure of quadrupole measurement is introduced. Each measurement requires preparation, calibration, alignment, and field content scan. Estimated time for single field content scan takes 15 seconds.

BIBLIOGRAPHY

[1] Marco Buzio. "Overview of Magnetic Measurements for Particle Accelerators". *International Magnetic Measurement Workshop 20*, 2017.

[2] L. Walckiers. "Magnetic measurements with coils and wires". 2011.

[3] A. Jain and R. Thomas. "Fiducialization and Calibration of Rotating Coil for Magnetic Measurement of the ERL Quadrupoles". Technical report, Brookhaven National Laboratory Magnet Division Note 646-11 (AM-MD-346), 2006.

[4] E. De Matteis, P. Arpaia, and S. Russenschuck. *"Magnetic field mapper based on rotating coil"*. PhD thesis, University degli Studi del Sannio and CERN, 2016.

[5] P. Arpaia, M. Buzio, R. De Oliveria, J. DiMarco, and G. Severino. "A high-precision miniaturized rotating coil transducer for magnetic measurements". *Sensor and Actuators A: Physical*, 2018.

[6] C. Doose. "Performance of rotating wire magnetic alignment system for the Advanced Photon Source Upgrade". *International Magnetic Measurement Workshop 20*, 2018.

[7] C. Doose and M.Kasa. "Multipole magnetic measurement using a lock-in Amplifier Technique". *North American Particle Accelerator Conference 2013*, 2013.

[8] Stephane Sanfilippo. "Challenges for the magnetic projects at the Paul Scherrer Institut". *International Magnetic Measurement Workshop 20*, 2018.

[9] Animesh Jain. "Harmonic Coils. *US particle accelerator school, Santa Babara, CA*, 2003.

[10] Animesh Jain. "Rotating Coil Measurement Errors*". *2nd Workshop on Beam Dynamics Meets Magnets (BeMa2014)*, 2014.

[11] Jack T. Tanabe. *"Iron Dominated Electromagnets"*. "World Scientific", 2005.

[12] Animesh Jain. "Magneti Design for Low Emittance Storage Rings". *MEDSI 2014*, 2014.

[13] J. Dimarco. "Fundamentals of Magnetic Measurement with Rotating Coils: A Tutorial". *International Magnetic Measurement Workshop 19*, 2015.

[14] B.C Brown, P.O. Mazur, J.F Ostiguy, S.M. Pruss, and F. Turkot. "Harmonic Analysis of Fermilab Main Ring Quadrupoles". *Fermilab-Conf-91/128*, 1991.

[15] F. Nicosia and J. Dimarco. "Magnetic field measurement system based on rotating PCB coils". 2014.

[16] Lloyd N. Trefethen and J.A.C Weideman. "The Exponentially Convergent Trapezoidal Rule". *SIAM Review*, 2014.

[17] Animesh Jain. "Harmonic Coils". *CERN Report 98-05, pp. 143-173*, 1997.

[18] MWS Wire Industries. *"MWS Wire Industries Copper Magnet Wire Data"*. `https://mwswire.com/magnet-wire/round-copper-magnet-wire/` Accessed: 2018-11-27.

[19] Newport Corporation. *"RGV100BL-S Data Sheet"*. `https://www.newport.com/mam/celum/celum_assets/resources/RGV100BL-S_Data_Sheet.pdf?1` Accessed: 2018-11-27.

[20] Newport Corporation. *"Trigger Synchronization using a Newport XPS Series Motion Controller"*. https://www.newport.com/medias/sys_master/images/images/hc9/h76/8797213327390/Motion-Tech-Note-Trigger-Synchronization-with-XPS-Controller.pdf Accessed: 2018-11-27.

[21] Stanford Research System. *"About Lock-In Amplifier"*.

[22] Zurich Instruments. *"HF2LI 50MHz Lock-in Amplifier"*. https://www.zhinst.com/sites/default/files/zi_hf2li_leaflet_web_0.pdf Accessed: 2018-11-27.

[23] National Instruments. *"NI PXIe 4309"*. http://www.ni.com/pdf/manuals/377030a.pdf Accessed: 2018-11-27.

[24] L. Walckiers, L. Bottura, M. Buzio, P. Schnizer, and N. Smirnov. "Sensitivity and Accuracy of the System for the Magnetic Measurement of the LHC Magnets at CERN". *Proceedings of EPAC 2000, Vienna, Austria*, 2000.

[25] SENIS Magnetic & current measurement. *"F3A Magnetic Field Transducers"*. http://c1940652.r52.cf0.rackcdn.com/5791e6b4ff2a7c38fb000a95/f3a-magnetic-transducer-datasheet_rev03.pdf Accessed: 2018-11-27.